J|A|C|S
ARTICLES
Published on Web 08/24/2007

Paclitaxel-Functionalized Gold Nanoparticles

Jacob D. Gibson, Bishnu P. Khanal, and Eugene R. Zubarev*

Contribution from the Department of Chemistry, Rice University, Houston, Texas 77005

Received July 12, 2007; E-mail: zubarev@rice.edu

Abstract: Here we describe the first example of 2 nm gold nanoparticles (Au NPs) covalently functionalized with a chemotherapeutic drug, paclitaxel. The synthetic strategy involves the attachment of a flexible hexaethylene glycol linker at the C-7 position of paclitaxel followed by coupling of the resulting linear analogue to phenol-terminated gold nanocrystals. The reaction proceeds under mild esterification conditions and yields the product with a high molecular weight, while exhibiting an extremely low polydispersity index (1.02, relative to linear polystyrene standards). TGA analysis of the hybrid nanoparticles reveals the content of the covalently attached organic shell as nearly 67% by weight, which corresponds to ~70 molecules of paclitaxel per 1 nanoparticle. The presence of a paclitaxel shell with a high grafting density renders the product soluble in organic solvents and allows for detailed ^{1}H NMR analysis and, therefore, definitive confirmation of its chemical structure. High-resolution TEM was employed for direct visualization of the inorganic core of hybrid nanoparticles, which were found to retain their average size, shape, and high crystallinity after multiple synthetic steps and purifications. The interparticle distance substantially increases after the attachment of paclitaxel as revealed by low-magnification TEM, suggesting the presence of a larger organic shell. The method described here demonstrates that organic molecules with exceedingly complex structures can be covalently attached to gold nanocrystals in a controlled manner and fully characterized by traditional analytical techniques. In addition, this approach gives a rare opportunity to prepare hybrid particles with a well-defined amount of drug and offers a new alternative for the design of nanosized drug-delivery systems.

Introduction

The difficulties associated with selective targeting of cancer cells have limited the success of modern chemotherapeutics. In addition, the hydrophobic nature of many anticancer drugs prevents the use of traditional modes of administration, which has proven to be equally problematic. However, significant progress in hydrophobic drug delivery has been reported, much of which is focused on encapsulation of drug molecules within the core of polymeric micelles[1−17] as well as dendrimers with hydrophilic shells.[18−20] Effective toward increasing the aqueous stability of many chemotherapeutic agents, more specifically paclitaxel, drug-carrier systems continue to rapidly gain interest. The relatively large sizes of these systems render them capable of exploiting the increased permeation and retention within tumors, thereby increasing the selective delivery of paclitaxel to cancerous tissue. Encapsulation methods, however, are not without intrinsic limitations as inefficient drug loading and clearance by the reticuloendothelial system (RES) remain a challenge.[1,4,5] Interestingly, it has been shown that smaller structures can evade RES capture and exhibit the ability to accumulate in a broader range of tumors creating a necessity for *nano-sized* delivery vehicles.[21−30]

(1) Farokhzad, O. C.; Cheng, J.; Teply, B. A.; Sherifi, I.; Jon, S.; Kantoff, P. W.; Richie, J. P.; Langer, R. *Proc. Natl. Acad. Sci. U.S.A.* **2006**, *103*, 6315−6320.
(2) Huang, H.; Remsen, E. E.; Kowalewski, T.; Wooley, K. L. *J. Am. Chem. Soc.* **1999**, *121*, 3805−3806.
(3) Hawker, C. J.; Wooley, K. L. *Science* **2005**, *309*, 1200−1205.
(4) Torchilin, V. P.; Lukyanov, A. N.; Gao, Z.; Papahadjopoulos-Sternberg, B. *Proc. Natl. Acad. Sci. U.S.A.* **2003**, *100*, 6039−6044.
(5) Gref, R.; Minamitake, Y.; Peracchia, M. T.; Trubetskoy, V.; Torchilin, V.; Langer, R. *Science* **1994**, *263*, 1600−1603.
(6) Oh, K. S.; Lee, K. E.; Han, S. S.; Cho, S. H.; Kim, D.; Yuk, S. H. *Biomacromolecules* **2005**, *6*, 1062−1067.
(7) Lee, H.; Zeng, F.; Dunne, M.; Allen, C. *Biomacromolecules* **2005**, *6*, 3119−3128.
(8) Sheihet, L.; Dubin, R. A.; Devore, D.; Kohn, J. *Biomacromolecules* **2005**, *6*, 2726−2731.
(9) Zhang, Z.; Feng, S.-S. *Biomacromolecules* **2006**, *7*, 1139−1146.
(10) Richard, R. E.; Schwarz, M.; Ranade, S.; Chan, A. K.; Matyjaszewski, K.; Sumerlin, B. *Biomacromolecules* **2005**, *6*, 3410−3418.
(11) Sipos, L.; Som, A.; Faust, R. *Biomacromolecules* **2005**, *6*, 2570−2582.
(12) Liang, H.-F.; Chen, S.-C.; Chen, M.-C.; Lee, P.-W.; Chen, C.-T.; Sung, H.-W. *Bioconjugate Chem.* **2006**, *17*, 291−299.
(13) Shuai, X.; Merdan, T.; Schaper, A. K.; Xi, F.; Kissel, T. *Bioconjugate Chem.* **2004**, *15*, 441−448.
(14) Menger, F. M.; Zhang, H.; de Joannis, J.; Kindt, J. T. *Langmuir* **2007**, *23*, 2308−2310.
(15) Gillies, E. R.; Jonsson, T. B.; Frechet, J. M. J. *J. Am. Chem. Soc.* **2004**, *126*, 11936−11943.
(16) O'Reilly, R. K.; Joralemon, M. J.; Wooley, K. L.; Hawker, C. J. *Chem. Mater.* **2005**, *17*, 5976−5988.
(17) Kwon, Y. J.; James, E.; Shastri, N.; Frechet, J. M. J. *Proc. Natl. Acad. Sci. U.S.A.* **2005**, *102*, 18264−18268.
(18) Ooya, T.; Lee, J.; Park, K. *Bioconjugate Chem.* **2004**, *15*, 1221−1229.
(19) Lee, C. C.; Yoshida, M.; Frechet, J. M. J.; Dy, E. E.; Szoka, F. C. *Bioconjugate Chem.* **2005**, *16*, 535−541.
(20) Hecht, S.; Frechet, J. M. J. *Angew. Chem., Int. Ed.* **2001**, *40*, 74−91.
(21) Hobbs, S. K.; Monsky, W. L.; Yuan, F.; Roberts, W. G.; Griffith, L.; Torchilin, V. P.; Jain, R. K. *Proc. Natl. Acad. Sci. U.S.A.* **1998**, *95*, 4607−4612.
(22) Karlsson, A. J.; Pomerantz, W. C.; Weisblum, B.; Gellman, S. H.; Palecek, S. P. *J. Am. Che. Soc.* **2006**, *128*, 12630−12631.
(23) Drummond, C. J.; Fong, C. *Curr. Opin. Colloid Interface Sci.* **1999**, *4*, 449−456.
(24) Kaasgaard, T.; Drummond, C. J. *Phys. Chem. Chem. Phys.* **2006**, *8*, 4957.
(25) Barauskas, J.; Johnsson, M.; Tiberg, F. *Nano Lett.* **2005**, *5*, 1615−1619.
(26) Loo, C.; Lowery, A.; Halas, N.; West, J.; Drezek, R. *Nano Lett.* **2005**, *5*, 709.

Attractive for their size, stability, and biocompatibility, gold nanoparticles (NPs) continue to gain interest due to their potential to enhance a number of biomedical applications.[31−49] More importantly, the ability to functionalize the surface of gold with organic molecules allows for the preparation of nanoparticles which can specifically interact with any physiological system.[50−58] Murray et al. reported on the use of ethidium thiolate modified Au NPs as a probe into the mechanism of DNA intercalation.[59] Similarly, Mirkin et al. have developed a method for the sequence-specific detection of polynucleotides based on DNA-functionalized Au nanoparticles.[60] Perhaps, attracting the most attention is the emerging application of surface modified Au NPs as vehicles for drug delivery. Recently, Paciotti et al. described the coating of 26 nm Au particles with a mixture of tumor necrosis factor (TNF), polyethylene glycol, and the chemotherapeutic paclitaxel as a multifunctional vector capable of targeted drug delivery to solid tumors.[61,62] Further increasing the potential of Au NP-based drug carriers, Rotello and co-workers have demonstrated the ability of thiol-functionalized particles to release ligands *in vivo* as a result of a glutathione-mediated place exchange reaction.[63,64]

Despite numerous examples detailing the coupling of biologically active compounds with AuNPs, observing and proving the presence of covalently bound molecules has been mainly limited to qualitative studies. In many cases only indirect methods can be used as an argument for successful covalent attachment because the power of solution characterization techniques (NMR, SEC, and LS) is often negated by low solubility and structural inhomogeneities of hybrid organic−inorganic structures. As a consequence, there exist very few reports on the preparation of organic−inorganic systems containing a specific number of drug molecules. In our previous work,[65,66] we have shown that polymer-functionalized metallic nanoparticles featuring a 2 nm gold core are, in fact, suitable for traditional characterization methods in solution and, therefore, present an attractive opportunity for manufacturing drug delivery vehicles with tunable properties. In this work we describe the synthesis of paclitaxel−gold nanoparticle hybrid structures in which the covalent attachment of paclitaxel molecules to the surface of 2 nm gold nanocrystals is observed using standard analytical techniques. The synthetic strategy described here yields a hybrid structure with an extremely high content of organic shell (67 wt. %), a narrow polydispersity index (1.02), and a *well-defined number* of drug molecules (73 ± 4) per metallic particle. This well-defined chemical structure of drug-functionalized nanoparticles may allow one to more accurately define their efficacy and therapeutic utility.

Results and Discussion

Preparation of the paclitaxel−AuNP conjugate begins with the synthesis of a linear analogue featuring a hydrophilic, carboxyl-terminated linker (hexaethylene glycol) anchored at the C-7 position of paclitaxel, which can be directly coupled to 4-mercaptophenol-functionalized 2 nm Au particles. Selection of the C7−OH group as the point of attachment was motivated by the structure−activity relationships reported for paclitaxel,[67−70] which show that chemical modification of this site does not cause any significant change in paclitaxel's ability to arrest cell division processes in cancer cells. This is in contrast to the C2′−OH group, the modification of which results in either drastic reduction or complete disappearance of biological activity. While reports on analogous paclitaxel compounds modified at the C2′−OH group exist,[71,72] these examples rely on enzymatic processes capable of unmasking this hydroxyl group *in vivo*. Furthermore,

(27) Hirsch, L. R.; Stafford, R. J.; Bankson, J. A.; Sershen, S. R.; Rivera, B.; Rrice, R. E.; Hazle, J. D.; Halas, N. J.; West, J. *Proc. Natl. Acad. Sci. U.S.A.* **2003**, *100*, 13549.
(28) Chithrani, B. D.; Chan, W. C. W. *Nano Lett.* **2007**, *7*, 1542−1550.
(29) Kam, N. W. S.; Liu, Z.; Dai, H. *Nanotechnology* **2006**, *45*, 577−581.
(30) Cheng, J. Y.; Wang, D. L.; Xi, J. F.; Au, L.; Siekkinen, A.; Warsen, A.; Li, Z. Y.; Zhang, H.; Xia, Y. N.; Li, X. D. *Nano Lett.* **2007**, *7*, 1318−1322.
(31) Alivisatos, P. *Nat. Biotechnol*. **2004**, *22*, 47−52.
(32) Medintz, I. L.; Konnert, J. H.; Clapp, A. R.; Stanish, I.; Twigg, M. E.; Mattoussi, H.; Mauro, J. M.; Deschamps, J. R. *Proc. Natl. Acad. Sci. U.S.A.* **2004**, *101*, 9612−9617.
(33) Simberg, D.; Duza, T.; Park, J. H.; Essler, M.; Pilch, J.; Zhang, L. L.; Derfus, A. M.; Yang, M.; Hoffman, R. M.; Bhatia, S.; Sailor, M. J.; Ruoslahti, E. *Proc. Natl. Acad. Sci. U.S.A.* **2007**, *104*, 932−936.
(34) Zhao, X.; Zhang, S. *Trends Biotechnol.* **2004**, *22* (9), 470−6.
(35) Lee, S. W.; Mao, C.; Flynn, C. E.; Belcher, A. M. *Science* **2002**, *296* (5569), 892−5.
(36) Everts, M.; Saini, V.; Leddon, J. L.; Kok, R. J.; Stoff-Khalili, M.; Preuss, M. A.; Millican, L. C.; Perkins, G.; Brown, J. M.; Bagaria, H.; Nikles, D. E.; Johnson, D. T.; Zharov, V. P.; Curiel, D. T. *Nano Lett.* **2006**, *6*, 587.
(37) Hainfeld, J. F.; Slatkin, D. N.; Smilowitz, H. M. *Phys. Med. Biol.* **2004**, *49*, N309−N315.
(38) Loo, C.; Hirsch, L.; Lee, M.-H.; Chang, E.; West, J.; Halas, N.; Drezek, R. *Optics Lett.* **2005**, *30*, 1012−1014.
(39) Nath, N.; Chilkoti, A. *Anal. Chem.* **2004**, *76*, 5370−5378.
(40) Pandey, P.; Singh, S. P.; Arya, S. K.; Gupta, V.; Datta, M.; Singh, S.; Malhotra, B. D. *Langmuir* **2007**, *23*, 3333−3337.
(41) Rothrock, A. R.; Donkers, R. L.; Schoenfisch, M. H. *J. Am. Chem. Soc.* **2005**, *127*, 9362−9363.
(42) Angelatos, A. S.; Radt, B.; Caruso, F. *J. Phys. Chem. B* **2005**, *109*, 3071−3076.
(43) Gole, A.; Murphy, C. J. *Langmuir*, **2005**, *21*, 10756−10762.
(44) Berry, V.; Gole, A.; Kundu, S.; Murphy, C. J.; Saraf, R. F. *J. Am. Chem. Soc.* **2005**, *127*, 17600−17601.
(45) Stone, J. W.; Sisco, P. N.; Goldsmith, E. C.; Baxter, S. C.; Murphy, C. J. *Nano Lett.* **2007**, *7*, 116−119.
(46) El-Sayed, I. H.; Huang, X.; El-Sayed, M. A. *Cancer Lett.* **2006**, *239*, 129−135.
(47) El-Sayed, I. H.; Huang, X.; El-Sayed, M. A. *Nano Lett.* **2005**, *5*, 829−834.
(48) Huang, X.; El-Sayed, I. H.; Qian, W.; El-Sayed, M. A. *J. Am. Chem. Soc.* **2006**, *128*, 2115−2120.
(49) Stoeva, S. I.; Lee, J.-S.; Smith, J. E.; Rosen, S. T.; Mirkin, C. A. *J. Am. Chem. Soc.* **2006**, *128*, 8378−8379.
(50) Templeton, A. C.; Wuelfing, W. P.; Murray, R. W. *Acc. Chem. Res.* **2000**, *33*, 27−36.
(51) Woehrle, G. H.; Brown, L. O.; Hutchison, J. E. *J. Am. Chem. Soc.* **2005**, *127*, 2172−2183.
(52) Cao, Y.; Jin, R.; Mirkin, C. A. *J. Am. Chem. Soc.* **2001**, *123*, 7961−7962.
(53) Liu, Y.; Shipton, M. K.; Ryan, J.; Kaufman, E. D.; Franzen, S.; Feldheim, D. L. *Anal. Chem.* **2007**, *79*, 2221−2229.
(54) Thanh, N. T. K.; Rosenzweig, Z. *Anal. Chem.* **2002**, *74*, 1624−1628.
(55) Peelle, B. R.; Krauland, E. M.; Wittrup, K. D.; Belcher, A. M.; *Langmuir* **2005**, *21*, 6929−6933.
(56) Murthy, V. S.; Cha, J. N.; Stucky, G. D.; Wong, M. S. *J. Am. Chem. Soc.* **2004**, *126*, 5292−5299.
(57) Hurst, S. J.; Lytton-Jean, A. K. R.; Mirkin, C. A. *Anal. Chem.* **2006**, *78*, 8313−8318.
(58) Claridge, S. A.; Goh, S. L.; Frechet, J. M. J.; Williams, S. C.; Micheel, C. M.; Alivisatos, A. P. *Chem. Mater.* **2005**, *17*, 1628−1635.
(59) Wang, G.; Zhang, J.; Murray, R. W. *Anal. Chem.* **2002**, *74*, 4320−4327.
(60) Elghanian, R.; Storhoff, J. J.; Mucic, R. C.; Letsinger, R. L.; Mirkin, C. A. *Science* **1997**, *277*, 1078−1081.
(61) Paciotti, G. F.; Kingston, D. G. I.; Tamarkin, L. *Drug. Dev. Res.* **2006**, *67*, 47−54.
(62) Paciotti, G. F.; Myer, L.; Weinreich, D.; Goia, D.; Pavel, N.; McLaughlin, R. E.; Tamarkin, L. *Drug Delivery* **2004**, *11*, 169−183.
(63) Hong, R.; Han, G.; Fernández, J. M.; Kim, B.-J.; Forbes, N. S.; Rotello, V. M. *J. Am. Chem. Soc.* **2006**, *128*, 1078−1079.
(64) Verma, A.; Simard, J. M.; Worrall, W. E.; Rotello, V. M. *J. Am. Chem. Soc.* **2004**, *126*, 13987−13991.
(65) Zubarev, E. R.; Xu, J.; Sayyad, A.; Gibson, J. D. *J. Am. Chem. Soc.* **2006**, *128*, 15098−15099.
(66) Khanal, B. P.; Zubarev, E. R. *Angew. Chem., Int. Ed.* **2007**, *46*, 2195−2198.
(67) Mathew, A. E.; Mejillano, M. R.; Nath, J. P.; Himes, R. H.; Stella, V. J. *J. Med. Chem.* **1992**, *35*, 145−151.
(68) Kingston, D. G. I. *Chem. Commun.* **2001**, 867−880.
(69) Deutsch, H. M.; Glinski, J. A.; Hernandez, M.; Haugwitz, R. D.; Narayanan, V. L.; Suffness, M.; Zalkow, L. H. *J. Med. Chem.* **1989**, *32*, 788−792.
(70) Nicolaou, K. C.; Riemer, C.; Kerr, M. A.; Rideout, D.; Wrasidlo, W. *Nature* **1993**, *364*, 464−466.
(71) Zakharian, T. Y.; Seryshev, A.; Sitharaman, B.; Gilbert, B. E.; Knight, V.; Wilson, L. J. *J. Am. Chem. Soc.* **2005**, *127*, 12508−12509.

Scheme 1. Synthesis of a Paclitaxel Analogue Featuring a Hexaethylene Glycol Linker at the C-7 Position

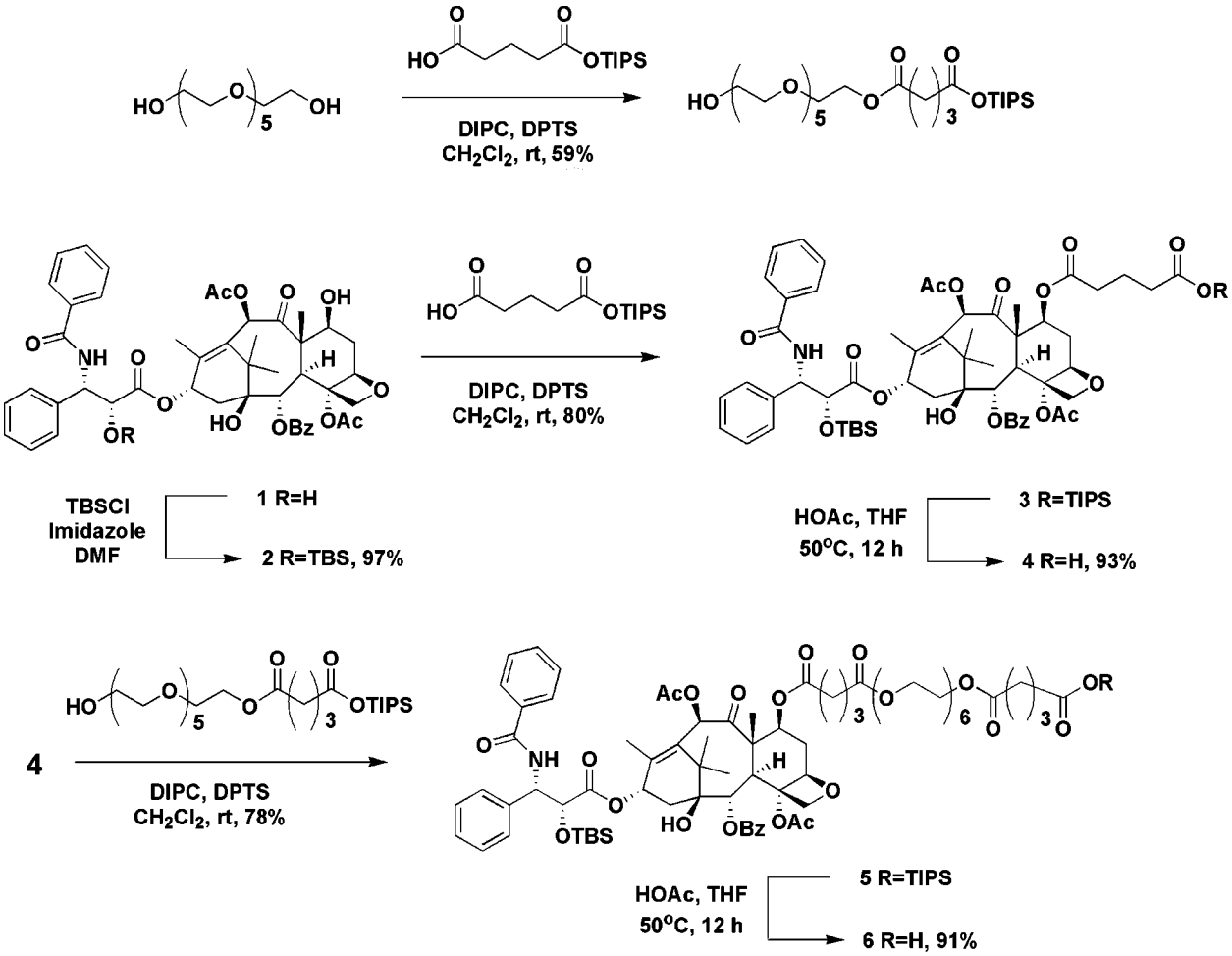

modifying the C-7 position is less likely to alter the biologically active T-shaped conformation, as defined by Kingston et al.[73] Incentive for the inclusion of hexaethylene glycol (HEG) into the structure of this linker is twofold in that (1) HEG increases the water solubility of the product, which can be further increased by introducing longer polyethylene glycol (PEG) linkers, and (2) the presence of multiple ethylene glycol units has been shown to minimize opsonization and RES clearance, hence increasing circulation time in the body.[74−78]

Selective protection of the ester-activated C2′−OH group of paclitaxel with *tert*-butyldimethylsilyl (TBS) chloride was carried out under standard conditions[78] to afford **2** with a 97% isolated yield. This approach gives exclusive access to the hydroxyl group located at the C-7 position because the C-1 tertiary hydroxyl is sterically hindered and remains unreactive under these mild conditions (Scheme 1). 1,3-Diisopropyl carbodiimide (DIPC) and 4-(*N*,*N*-dimethylamino)pyridinium-4-toluenesulfonate (DPTS) have been shown to effect esterification in high yields and represent the standard coupling agents described in this sequence.[79,80] Introduction of a carboxylic acid functionality at the C-7 position was achieved upon the coupling of **2** with glutaric acid monotriisopropylsilyl (TIPS) ester followed by selective cleavage of the TIPS group using acetic acid in THF at slightly elevated temperatures (50 °C). Importantly, under these conditions C2′−OTBS remains intact as confirmed by ^{1}H NMR analysis (see Supporting Information). Acetic acid has been shown to minimize the formation of side products when used in the synthesis of paclitaxel.[81]

In a separate synthesis, the hexaethylene glycol (HEG) portion of the linker was prepared by coupling excess HEG (5 mol equiv) with glutaric acid monotriisopropylsilyl ester in the presence of DIPC/DPTS, which was then reacted with compound **4** under the same esterification conditions to give the desired product **5** in 78% isolated yield. Again, acetic acid was employed to selectively cleave the TIPS group, providing a TBS-protected paclitaxel analogue **6**, which features a carboxyl-terminated HEG linker. Interestingly, we were able to take advantage of paclitaxel's poor solubility profile, as several

(72) Safavy, A.; Bonner, J. A.; Waksal, H. W.; Buchsbaum, D. J.; Gillespie, G. Y.; Khazaeli, M. B.; Arani, R.; Chen, D.-T.; Carpenter, M.; Raisch, K. P. *Bioconjugate Chem.* **2003**, *14*, 302−310.
(73) Ganesh, T.; Yang, C.; Norris, A.; Glass, T.; Bane, S.; Ravindra, R.; Banerjee, A.; Metaferia, B.; Thomas, S. L.; Giannakakou, P.; Alcaraz, A. A.; Lakdawala, A. S.; Snyder, J. P.; Kingston, D. G. I. *J. Med. Chem.* **2007**, *50*, 713−725.
(74) Mishra, S.; Webster, P.; Davis, M. E. *Eur. J. Cell Biol.* **2004**, *83*, 97−111.
(75) Moghimi, S. M. *Biochim. Biophys. Acta* **2002**, *1590*, 131−139.
(76) Gabizon, A. A. *Clin. Cancer Res.* **2001**, *7*, 223−225.
(77) Remaut, K.; Lucas, B.; Raemdonck, K.; Braeckmans, K.; Demeester, J.; De Smedt, S. C. *Biomacromolecules* **2007**, *8*, 1333−1340.
(78) Magri, N. F.; Kingston, D. G. I. *J. Nat. Prod.* **1988**, *51*, 298−306.
(79) Moore, J. S.; Stupp, S. I. *Macromolecules* **1990**, *23*, 65−71.
(80) Teng, J.; Zubarev, E. R. *J. Am. Chem. Soc.* **2003**, *125*, 11840−11841.
(81) Singh, A. K.; Weaver, R. E.; Powers, G. L.; Rosso, V. W.; Wei, C.; Lust, D. A.; Kotnis, A. S.; Comezoglu, F. T.; Liu, M.; Bembenek, K. S.; Phan, B. D.; Vanyo, D. J.; Davies, M. L.; Mathew, R.; Palaniswamy, V. A.; Li, W.-S.; Gadamsetti, K.; Spagnuolo, C. J.; Winter, W. J. *Org. Process Res. Dev.* **2003**, *7*, 25−27.

Scheme 2. Covalent Coupling of Paclitaxel to 4-Mercaptophenol-Modified 2 nm Gold Nanoparticles

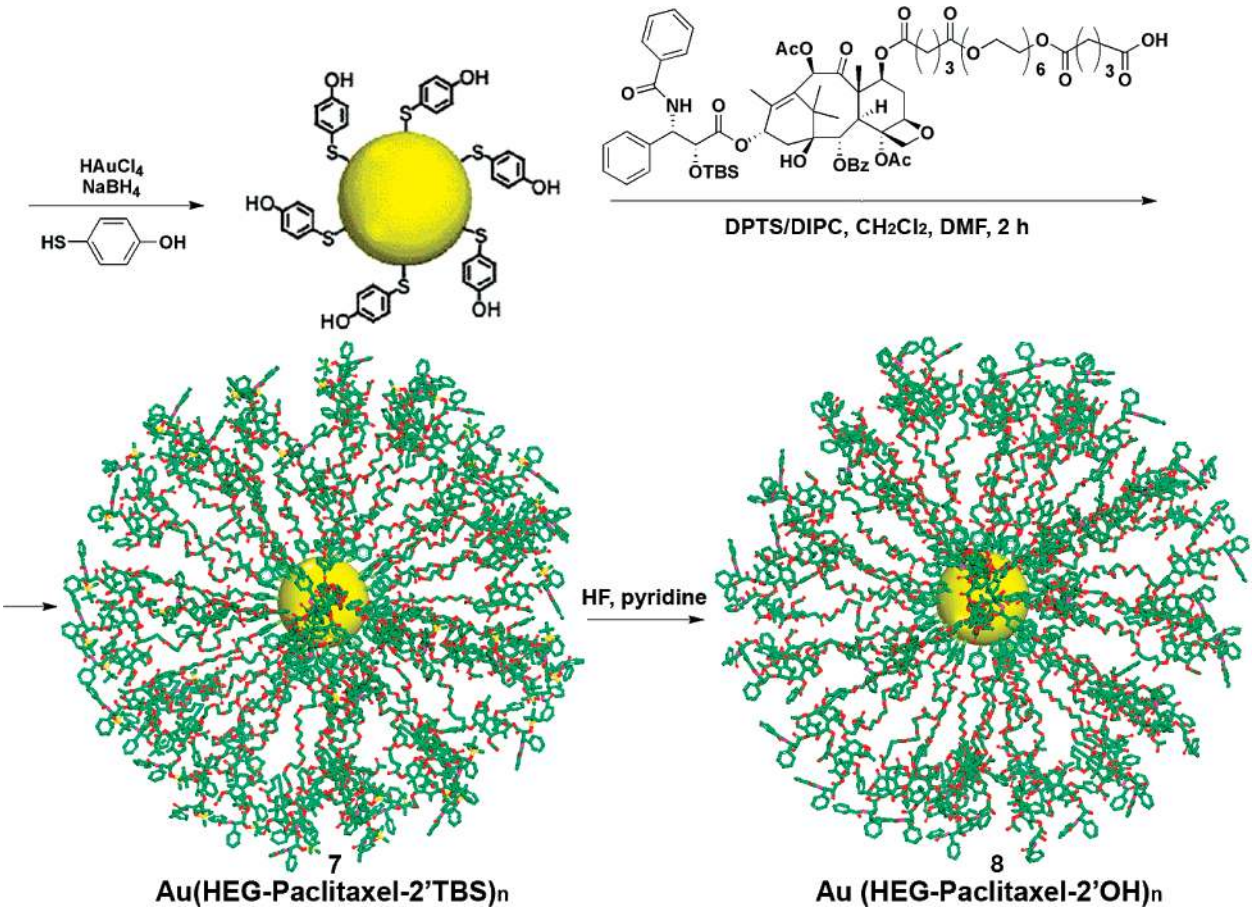

intermediates (**2**, **4**, and **6**) are not soluble in nonpolar solvents, allowing for the clean precipitation of the product from hexane as a common protocol for purification.

Standard conditions were employed for the coupling of TBS-protected paclitaxel derivative **6** and 4-mercaptophenol-functionalized Au nanoparticles (Scheme 2), which were prepared using a modified procedure introduced by Brust and coworkers.[82] However, dropwise addition of 30% DMF to a methylene chloride suspension of Au NPs is required to bring the hydroxyl-terminated particles into solution as they are not readily soluble in nonpolar solvents. The progress of this reaction is easily monitored, as the nature of **7** renders the system compatible with size exclusion chromatography (SEC). SEC traces taken after 2 h show near complete consumption of **6** and the presence of a high molar mass peak with a very low polydispersity index (PDI = 1.02) corresponding to TBS-protected paclitaxel-functionalized gold nanoparticles **7** (Figure 1). This remarkably low value of PDI is in good agreement with DLS data (see Figure S19) and suggests a nearly monodisperse size of hybrid nanoparticles in solution as well as a uniform distribution of paclitaxel molecules along their surfaces. However, some underestimation of the polydispersity is possible because SEC relies on a calibration curve based on linear polymer standards.

Similarly, the molar mass of hybrid nanoparticles **7** measured by SEC relative to polystyrene standards is highly underestimated, as the molecular weight of 2 nm gold clusters alone is at least 53 000 Da (~270 Au atoms). In addition, SEC analysis is known to underestimate the molecular weight of branched structures, i.e., dendrimers and star-shaped polymers, when the hydrodynamic radii of linear standards are used for calibration.[83] Chromatograms taken after 4 and 8 h reveal similar ratios of product to starting material, suggesting that the maximum

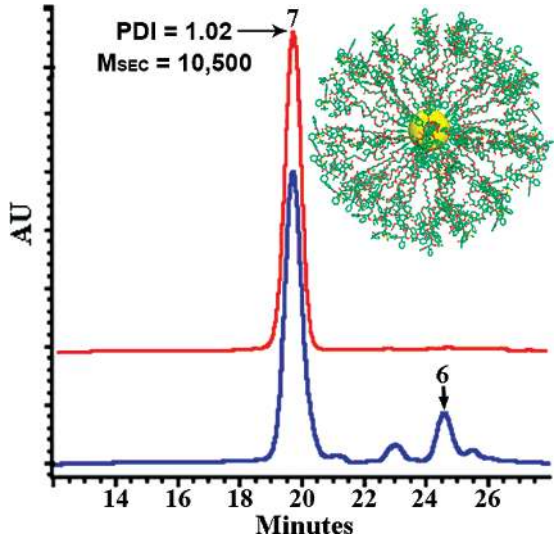

Figure 1. Size exclusion chromatography traces (eluting with THF) showing the coupling of compound **6** to the surface of Au NPs (bottom), and the isolated product **7** after purification (top). See also Figure S20 in the Supporting Information for SEC traces of pure compound **6** and final product **8**.

(82) Brust, M.; Fink, J.; Bethell, D.; Schiffrin, D. J.; Kiely, C. *J. Chem. Soc., Chem. Commun.* **1995**, 1655.

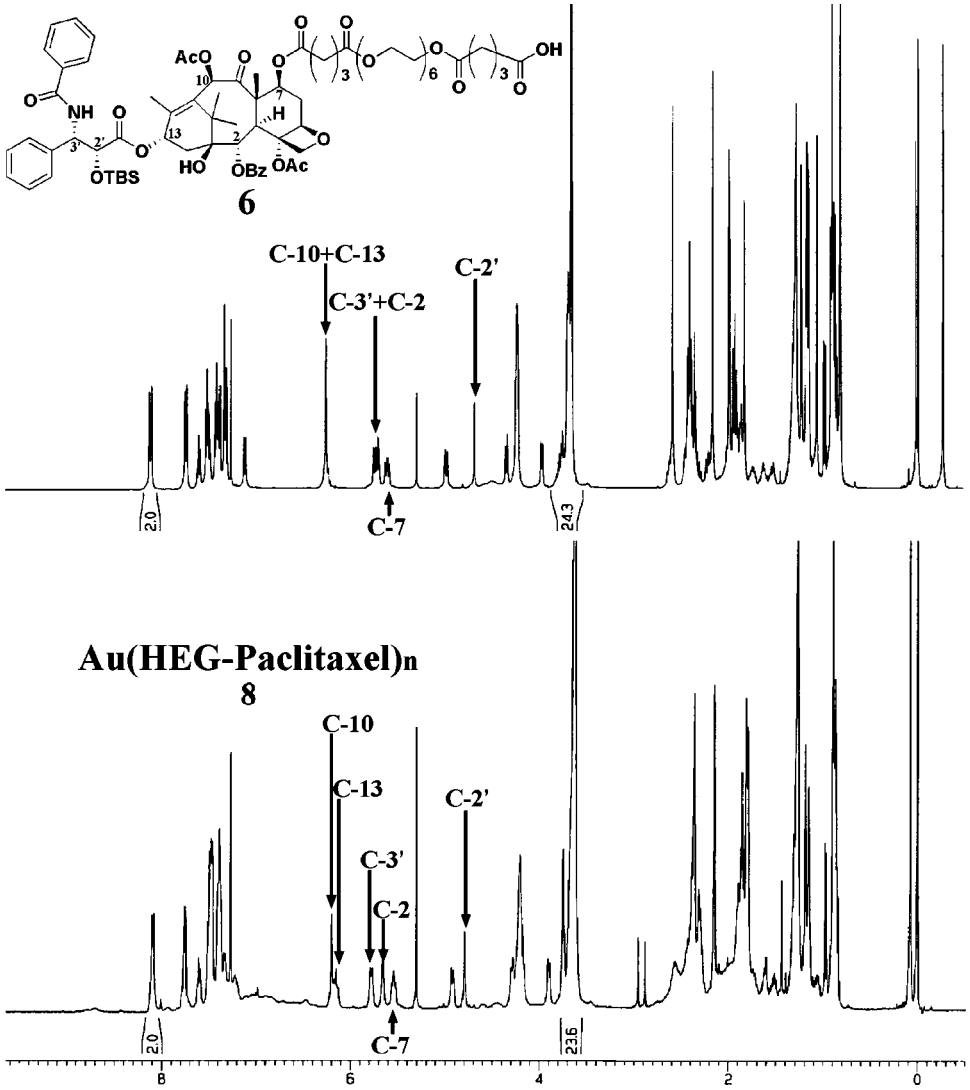

Figure 2. ^{1}H NMR spectra of paclitaxel analogue **6** (top) and the isolated hybrid structure **8** (bottom).

possible amount of **6** is coupled to AuNPs within the first 2 h. Purification of the product **7** is equally simplified, as its much larger size can be exploited by centrifugal ultrafiltration. DMF solutions of the reaction mixture were placed on regenerated cellulose membranes with MWCO 30 kDa and centrifuged at 3750 rpm. Only three 45-min rounds of centrifugation were necessary for the complete removal of all starting materials as determined by SEC (Figure 1, top). Last, the synthesis of the paclitaxel−AuNP conjugate **8** was complete upon liberation of the C2′−OH groups of paclitaxel moieties using HF in pyridine (70:30 v/v, respectively), followed by precipitation from hexane affording **8** as a gray-brown powder.

Upon purification, the successful coupling of paclitaxel to Au nanoparticles was confirmed by ^{1}H NMR (see also Figure S18 for IR spectra). Figure 2 details the proton spectra for paclitaxel−HEG analogue **6** (top) and the final product **8** (bottom). The overall appearance, position, and the integration values of all major signals are very similar. In both cases, the integration ratio of paclitaxel aromatic protons, for example, the C-23, C-27 doublet at 8.11 ppm, to HEG nonterminal aliphatic protons at 3.65 ppm remains the same (2H vs 24H). In addition, the location of a triplet corresponding to the C-7 proton in both products **6** and **8** is at 5.6 ppm (Figure 2), which is very different from that of free paclitaxel where the C-7 proton appears at 4.4 ppm (see Supporting Information). Because this triplet integrates exactly as 1H, one can conclude that all paclitaxel moieties in product **8** are attached to the glutaric acid-HEG linker. The linker, in turn, must be connected to gold nanoparticles because SEC analysis of **8** demonstrated the complete absence of precursor **6** or any other low molar mass species (Figure 1, top). On the other hand, there are distinct differences in the two spectra presented in Figure 2. Nearly all signals from the final product **8** are broader compared to those of **6**, which is indicative of the decreased rotational mobility of paclitaxel moieties covalently attached to the surface of gold nanocrystals. Most affected by this phenomenon are those signals associated with HEG (4H at 4.2 ppm and 22H at 3.65 ppm) and glutaric acid (1.7−2.4 ppm), lending to their closer proximity to the gold surface.

It is important to emphasize, however, that the presence of the highly flexible and relatively long HEG linker is crucial for the NMR characterization of paclitaxel-functionalized nanoparticles. Our control experiment showed that nearly all resonances become exceedingly broad and unrecognizable if

(83) Mourey, T. H.; Turner, S. R.; Rubinstein, M.; Frechet, J. M. J.; Hawker, C. J.; Wooley, K. L. *Macromolecules* **1992**, *25*, 2401−2406.

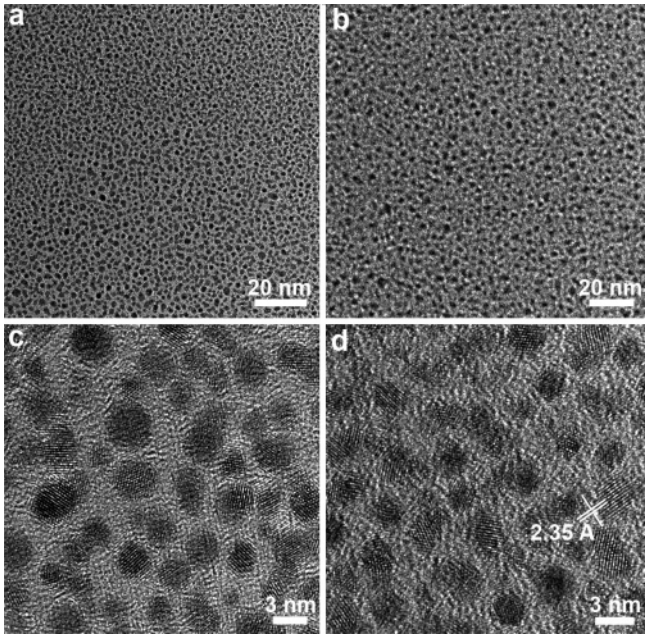

Figure 3. TEM and HRTEM images of 4-mercaptophenol-coated Au NPs (a, c) and paclitaxel-functionalized Au NPs (b, d).

paclitaxel is directly coupled to the surface of AuNPs (without the HEG linker). Another important feature of the NMR spectrum collected from **8** is a very broad signal in the range between 7.2 and 6.7 ppm. This is due to the presence of 4-mercaptophenol ligands, which connect paclitaxel−HEG chains to the surface of AuNPs. The broad signal appears only after the attachment, and it is not present in the starting material **6**. Finally, several fine changes in the spectra prove complete deprotection of the C2′−OH group. First, the signals of TBS methyl groups (0 and −0.3 ppm) and the *tert*-butyl group (0.8 ppm) are not observed in the spectrum of the final product **8**. Second, the resonances of protons attached to C-2′ and C-3′ undergo slight shifts downfield from 4.65 to 4.82 ppm and from 5.7 to 5.8 ppm, respectively (Figure 2). Additionally, a small upfield shift of the C-13 proton takes place upon deprotection, and the signal is no longer overlapped with that of the C-10 proton as in the case of precursor **6**. This slight separation of C-10 and C-13 signals was only observed in the final product **8** and in the unprotected paclitaxel, whereas the NMR spectra of all TBS-protected intermediates **2** through **7** showed a complete overlap of these particular peaks (see Supporting Information).

In order to confirm that the soluble product **8** with a high molecular weight (SEC) and an NMR spectrum similar to that of precursor **6** is indeed a hybrid organic−inorganic structure, we performed several TEM experiments. First, we imaged the starting 2 nm gold nanoparticles coated with 4-mercaptophenol. Figure 3a shows a low magnification TEM image of AuNPs deposited from a THF solution onto a carbon-coated grid. The average size of the particles is close to 2 nm, although structures as small as 0.7 nm and as big as 4.3 nm can be found in the image. The interparticle distance also varies within a relatively large range (0.5 to 3 nm), but the average value is close to 1 nm, which is in good agreement with earlier reports.[82] Importantly, TEM imaging of the final product **8** reveals the presence of spherical particles with a very similar average size of ∼2 nm (Figure 3b), which implies that, during the coupling of compound **6** and the deprotection of nanoparticles **7**, Oswald ripening of metallic cores did not occur. However, the interparticle distance is substantially increased (∼2.5 nm), indicating the presence of a much larger organic shell. This distance is approximately twice the size of a paclitaxel molecule, but it is shorter than the length of compound **6** in its fully extended conformation (4.6 nm). High flexibility and a small cross-sectional area of HEG chains may explain this difference. It is reasonable to expect that drying would cause HEG linkers to collapse near the surface of the gold core. In addition, the interdigitation of ligands from adjacent nanocrystals may take place in accord with the observations reported for alkanethiolate gold clusters.[84−87]

The conventional bright-field TEM, however, does not prove that the dark spherical objects shown in Figure 2a and 2b are indeed gold nanocrystals. For that purpose we employed high-resolution TEM imaging of both mercaptophenol- and paclitaxel-functionalized nanoparticles **8** (Figure 3c,d). The majority of particles exhibit the characteristic lattice fringes, which represent the individual atomic layers. The *d*-spacing between the fringes is either 2.04 or 2.35 Å, which allows one to identify them as {200} and {111} crystallographic planes of *fcc* Au and offers definitive proof that these structures are crystalline. Most of the particles are single crystals, and only occasional twinning of particles is observed. Importantly, HRTEM clearly demonstrates that the average size of particles, and their degrees of crystallinity have not been altered during the multistep synthesis and several ultrafiltration steps en route to the final product **8**. Figure 3d also shows that the metallic cores of hybrid structures **8** have near-spherical shapes, which simplifies the estimation of the number of organic molecules attached and their grafting density, as discussed below.

The number of paclitaxel molecules attached to each Au particle was first determined qualitatively from the weight gain observed upon isolation of paclitaxel-functionalized nanoparticles **8**. Based on the mass of product (24 mg) formed from the starting Au NPs (9.5 mg), one can estimate that the mass increase is approximately 150% by weight, which is due to the covalent attachment of HEG-paclitaxel moieties. It has been previously reported that 2 nm gold clusters contain ∼270 atoms[88,89] (M_{Au} = 53 000 Da) and the number of thiol ligands protecting their surface is approximately 126 based on TGA (see below). The molecular weight of mercaptophenol-coated particles is then 68 750 Da (M_{Au} + 126·$M_{C_6H_5OS}$), and the increase of 150% corresponds to ∼103 125 Da. Given the molecular weight of **6** (1342 g/mol, without TBS), there are on average 103 125/1342 ≅ 77 paclitaxel molecules per one Au NP. However, this estimation assumes a quantitative conversion of starting Au nanoparticles to product **8**.

(84) Terrill, R. H.; Postlethwaite, T. A.; Chen, C.-H.; Poon, C.-D.; Terzis, A.; Chen, A.; Hutchison, J. E.; Clark, M. R.; Wignall, G.; Londono, J. D.; Superfine, R.; Falvo, M.; Johnson, C. S., Jr.; Samulski, E. T.; Murray, R. W. *J. Am. Chem. Soc.* **1995**, *117*, 12537−12548.
(85) Badia, A.; Singh, S.; Demers, L.; Cuccia, L.; Brown, G. R.; Lennox, R. B. *Chem.—Eur. J.* **1996**, *2*, 359−363.
(86) Whetten, R. L.; Khoury, J. T.; Alvarez, M. M.; Murthy, S.; Vezmar, I.; Wang, Z. L.; Stephens, P. W.; Cleveland, C. L.; Luedtke, W. D.; Landman, U. *Adv. Mater.* **1996**, *8*, 428−433.
(87) Ohara, P. C.; Leff, D. V.; Heath, J. R.; Gelbart, W. M. *Phys. Rev. Lett.* **1995**, *75*, 3466−3469.
(88) Daniel, M.-C.; Astruc, D. *Chem. Rev.* **2004**, *104*, 293−346.
(89) Hostetler, M. J.; Wingate, J. E.; Zhong, C.; Harris, J. E.; Vachet, R. W.; Clark, M. R.; Londono, J. D.; Green, S. J.; Stokes, J. J.; Wignall, G. D.; Glish, G. L.; Porter, M. D.; Evans, N. D.; Murray, R. W. *Langmuir* **1998**, *14*, 17−30.

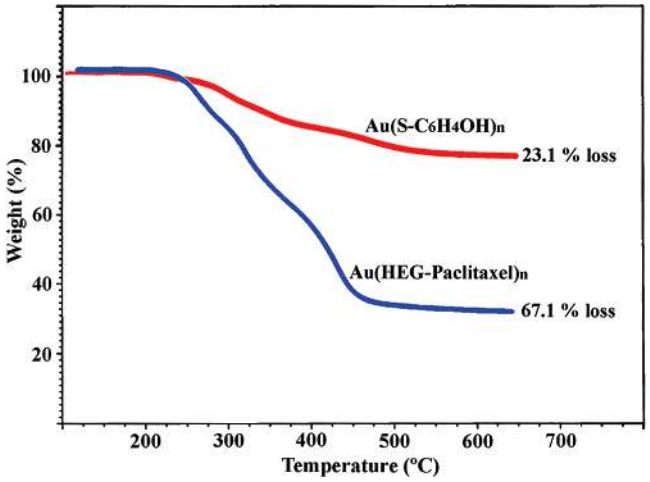

Figure 4. TGA data measuring the loss of organic material corresponding to 4-mercaptophenol-coated Au NPs (red) and hybrid structure **8** (blue).

In order to corroborate the calculated number of paclitaxel molecules, **8** was subjected to thermogravimetric (TGA) analysis which allows for direct measurement of the weight content of organic shell. As a control, 4-mercaptophenol-functionalized Au NPs were first analyzed in order to measure the amount of organic material (mercaptophenol ligands) present before the coupling of **6**. The result of this experiment reveals that thiol ligands account for approximately 23.1% of the mass of stock Au NPs (Figure 4, top). Coupled with the molar mass of mercaptophenol (125 g/mol), each Au particle was found to contain 126 functional sites. Using this same procedure, the composition of **8** was determined to be 67.1% organic and 32.9% metallic Au. Since the molecular weight of the gold core is 53 kDa, the total molecular weight of organic shell is then 108 kDa. Assuming that the number of mercaptophenol ligands remained constant, the molecular weight of HEG−paclitaxel moieties is 92.3 kDa (108 000 − 126·$M_{C_6H_5OS}$), which gives approximately 69 molecules per particle. This remarkable agreement between the TGA data and the estimation based on the mass gain upon coupling reaction indicates the reliability and high accuracy of both methods. These results also reveal the high efficiency of the synthetic strategy used for the preparation of hybrid structures described here. To the best of our knowledge, the organic content (67.1 wt %) in nanoparticles **8** is the highest value reported for any hybrid structures to date. It significantly exceeds the records reported for polymer-functionalized Au NPs with a high grafting density (56.5%).[90] Therefore, our approach allows for the preparation of core−shell nanostructures, which are well-defined in terms of their size, the content of the organic layer, and the number of molecules grafted to the inorganic core. Most importantly, one can use this strategy to prepare hybrid systems with a high drug loading capacity.

Conclusion

A novel approach toward the preparation of a well-defined drug−gold nanoparticle system has been described. The resulting hybrid structure is unique in that the small ratio of gold core to organic shell allows for both solution and solid-state characterization based on powerful analytical techniques. Such an analysis reveals a system containing a well-defined number of paclitaxel molecules with near uniform composition, as evidenced by SEC, NMR, TEM, and TGA experiments. Perhaps most importantly, this approach allows for a more accurate measurement of biological activity as a result of the increased ability to quantify the amount of drug present. An investigation into the biological activity of this system is ongoing and will be reported in due course.

(90) Corbierre, M. K.; Cameron, N. S.; Lennox, R. B. *Langmuir* **2004**, *20*, 2867−2873.

Experimental Section

Unless otherwise stated, all starting materials were obtained from commercial suppliers and used without further purification. ^{1}H NMR spectra were recorded in $CDCl_3$ using a Bruker 400 MHz spectrometer. Size Exclusion Chromatography (SEC) analysis was performed on a Waters Breeze 1515 series liquid chromatograph equipped with a dual λ absorbance detector (Waters 2487), automatic injector, and three styrogel columns (HR1, HR3, HR4) using linear polystyrene standards for the calibration curve and tetrahydrofuran (THF) as the mobile phase. Thermogravimetric analysis was performed on a TA Instruments TGA Q50. Samples (3.0−6.0 mg) were placed in platinum sample pans and heated under an argon atmosphere at a rate of 10 °C/min to 100 °C and held for 30 min to completely remove residual solvent. Samples were then heated to 700 °C at a rate of 10 °C/min. TEM and HRTEM imaging were performed on a JEOL 2100F transmission electron microscope operating at 200 kV accelerating voltage. Samples were drop cast from dilute solutions of 10% THF in CH_2Cl_2 onto carbon-coated TEM grids and allowed to dry in open air. Centrifugal filters (2 mL capacity) Ultrafree-CL containing regenerated cellulose membranes with a molecular weight cutoff of 30 000 g/mol were purchased from Fisher Scientific Inc. 4-(*N*,*N*-Dimethylamino)pyridinium-4-toluenesulfonate (DPTS) was prepared by mixing saturated THF solutions of *N*,*N*-dimethylaminopyridine (DMAP) (1 equiv) and *p*-toluenesulfonic acid monohydrate (1 equiv) at room temperature. The precipitate was filtered, washed several times with THF, and dried under vacuum.

Glutaric Acid Mono-triisopropylsilyl Ester. Triisopropylsilyl chloride (TIPSCl) (3.2 g, 16.6 mmol) was introduced dropwise into a solution of 2.0 g (15.1 mmol) of glutaric acid in 25 mL of DMF. The reaction vessel was then equipped with a rubber septum, and under rigorous agitation, 1.45 g (16.5 mmol) morpholine were slowly injected via syringe. After 5 min the reaction was stopped by diluting the mixture 5-fold with dichloromethane, removing DMF and morpholine by washing the organic solution 4 times with DI water followed by one extraction using an aqueous solution of 3% citric acid. The solvent was then reduced on a rotary evaporator at 40 °C, and the crude product was purified by column chromatography using 5% THF/CH_2Cl_2 as an eluent (R_f = 0.60). The result was a colorless oil with a typical yield of 1.70 g (39%). ^{1}H NMR (400 MHz, $CDCl_3$) δ 1.06 (d, 18H)[a], 1.30 (m, 3H)[b], 1.95 (m, 2H), 2.44 (t, 4H); ^{13}C NMR (100 MHz, $CDCl_3$) δ 12.17, 17.64, 20.08, 33.09, 34.69, 172.99, 179.24; IR (neat) ν_{max} 2948, 1716, 1211, 1060, 1001, 883, 684 cm^{-1}; SEC (254 nm, THF): M_{SEC} = 236; PDI = 1.005.

Glutaric Acid Triisopropylsilyl Ester Hexaethylene Glycol Ester. Mono-TIPS-glutaric acid (0.5 g, 1.7 mmol), hexaethylene glycol (2.5 g, 8.85 mmol), and DPTS (0.8 g, 2.7 mmol) were dissolved in 30 mL of dichloromethane. After all components were in solution, 1 mL (7.7 mmol) of DIPC was added. Complete consumption of starting TIPS-glutaric acid was observed by GPC after 2 h. The reaction was stopped by diluting with dichloromethane and removing DPTS via five extractions with DI water. The organic fraction was reduced, and the product isolated by column chromatography eluting with 20% THF/CH_2Cl_2 (R_f = 0.40). Yield 0.568 g (59%). ^{1}HNMR ($CDCl_3$) δ 1.06 (d, 18H)[a], 1.27 (m, 3H)[b], 1.93 (m, 2H), 2.40 (t, 4H), 3.67 (m, 22H), 4.21 (m, 2H); ^{13}C NMR (100 MHz, $CDCl_3$) δ 11.86, 17.75, 20.33, 23.46, 33.20, 34.76, 61.66, 63.51, 69.10, 70.52, 72.62, 172.97; IR (neat) ν_{max} 3479, 2867, 1733, 1652, 1464, 1418, 1384, 1142, 949, 884, 744, 685 cm^{-1}; SEC (254 nm, THF): M_{SEC} = 378; PDI = 1.002.

2′-OTBS-paclitaxel (2). A stock silylating solution was prepared by dissolving *tert*-butyldimethylsilyl chloride (TBSCl) (0.57 g, 3.8 mmol) and imidazole (7.6 mmol, 0.52 g) in 1.0 mL of dry DMF. Please note that the final volume of the silylating solution was more than 1.0 mL. A 0.50 mL aliquot of this stock solution was then used to dissolve 100 mg (0.12 mmol) of paclitaxel. The reaction was monitored by TLC using 1:1 (v/v) hexane/EtOAc as an eluent (product $R_f = 0.40$). The complete disappearance of starting Taxol ($R_f = 0.10$) was observed after 30 min, and the reaction was quenched by diluting with dichloromethane and extracting DMF and imidazole with DI water. The remaining dichloromethane solution was concentrated, and precipitation from hexane provided 110 mg of the final product as a white powder. Yield 97%. ^{1}H NMR ($CDCl_3$) δ −0.27 (s, 3H)[c], −0.03 (s, 3H)[c], 0.81 (s, 9H)[c], 1.14 (s, 3H), 1.25 (s, 3H), 1.69 (s, 3H), 1.91−1.93 (broad, 4H), 2.15 (m, 1H), 2.23 (s, 3H), 2.45 (m, 1H), 2.57−2.58 (broad, 4H), 3.83 (d, 1H), 4.24 (d, 1H), 4.32 (d, 1H), 4.40 (m, 1H), 4.67 (s, 1H), 5.00 (d, 1H), 5.69 (d, 1H), 5.72 (m, 1H), 6.30 (broad, 2H), 7.09 (d, 1H), 7.33 (m, 3H), 7.41 (m, 4H), 7.50 (m, 3H), 7.60 (m, 1H), 7.74 (d, 2H), 8.13 (d, 2H); ^{13}C NMR (100 MHz, $CDCl_3$) δ −5.79, −5.25, 9.65, 14.95, 18.17, 20.85, 22.31, 23.06, 25.54, 26.78, 35.60, 35.83, 43.26, 45.54, 55.69, 58.52, 71.43, 72.13, 75.11, 75.56, 79.13, 81.16, 84.46, 126.45, 127.01, 128.03, 128.79, 129.18, 130.24, 131.83, 132.95, 133.68, 134.07, 138.27, 142.44, 167.01, 170.14, 171.28, 171.38, 203.76; IR (neat) ν_{max} 3441, 2930, 1733, 1652, 1581, 1125, 744 cm^{-1}; SEC (254 nm, THF): $M_{SEC} = 490$; PDI = 1.003.

Compound 3. Compound **2** (160 mg, 0.17 mmol), mono-TIPS-glutaric acid (75 mg, 0.26 mmol), and DPTS (100 mg, 0.33 mmol) were placed in a small vial and dissolved in 2.0 mL of dichloromethane. Upon stirring for 5 min, DIPC (100 mg, 0.79 mmol) was added dropwise to initiate coupling. After 4 h, the absence of starting **2** was observed by GPC. The reaction was stopped via 5-fold dilution of the reaction mixture with dichloromethane and four water extractions to remove DPTS. The crude product was purified by column chromatography using 2:1 (v/v) hexane/EtOAc as an eluent ($R_f = 0.60$). The yield for this reaction was 163 mg (80%). ^{1}H NMR ($CDCl_3$) δ −0.29 (s, 3H)[c], −0.01 (s, 3H)[c], 0.81 (s, 9H)[c], 1.07 (broad, 18H)[a], 1.17 (s, 3H)[b], 1.22 (m, 3H), 1.82−1.95 (m, 6H), 1.99 (s, 3H), 2.15−2.20 (broad, 4H), 2.35−2.45 (m, 5H), 2.58 (broad, 4H), 3.95 (d, 1H), 4.23 (d,1H), 4.34 (d, 1H), 4.68 (s, 1H), 4.95 (d, 1H), 5.65 (t, 1H), 5.72 (m, 2H), 6.28 (broad, 2H), 7.09 (d, 1H), 7.33 (m, 3H), 7.43 (m, 4H), 7.51 (m, 3H), 7.62 (m, 1H), 7.75 (d, 2H), 8.13 (d, 2H). SEC (254 nm, THF): $M_{SEC} = 690$; PDI = 1.004.

Compound 4. A 5.6 mL aliquot of glacial acetic acid was added to a solution containing 150 mg (0.12 mmol) of **3** in 2.0 mL of THF. After the dropwise addition of 0.40 mL of H_2O, the reaction mixture was heated to 50 °C. The reaction was monitored by TLC eluting with 2:1 (v/v) hexane/EtOAc. After 12 h, the complete conversion of carboxyl protected compound ($R_f = 0.60$) to the free carboxyl product ($R_f = 0.10$) was observed. The reaction mixture was diluted with dichloromethane and washed 5 times with DI water. The organic fraction was reduced on a rotary evaporator at 40 °C, and precipitation from hexane yielded 122 mg (93%) as a white solid. ^{1}H NMR ($CDCl_3$) δ −0.28 (s, 3H)[c], −0.02 (s, 3H)[c], 0.81 (s, 9H)[c], 1.22 (m, 3H), 1.82−1.90 (m, 6H), 1.99 (s, 3H), 2.15−2.20 (broad, 4H), 2.33−2.45 (m, 5H), 2.58 (broad, 4H), 3.95 (d, 1H), 4.23 (d, 1H), 4.34 (d, 1H), 4.68 (s, 1H), 5.00 (d, 1H), 5.65 (t, 1H), 5.72 (m, 2H), 6.28 (broad, 2H), 7.09 (d, 1H), 7.33 (m, 3H), 7.43 (m, 4H), 7.51 (m, 3H), 7.62 (m, 1H), 7.75 (d, 2H), 8.13 (d, 2H); ^{13}C NMR (100 MHz, $CDCl_3$) δ −5.81, −5.18, 10.91, 12.29, 14.61, 17.70, 18.14, 19.39, 20.69, 21.43, 23.01, 23.33, 25.54, 26.37, 32.88, 33.39, 35.55, 42.35, 43.37, 46.83, 55.70, 56.04, 71.32, 74.58, 75.07, 78.51, 81.01, 84.00, 126.42, 127.03, 128.01, 128.78, 129.18, 130.22, 131.89, 132.79, 133.70, 134.05, 138.18, 140.84, 166.83, 167.39, 169.04, 169.87, 171.53, 172.12, 177.60, 201.99; IR (neat) ν_{max} 3435, 2952, 2861, 2253, 1733, 1652, 1580, 1520, 1486, 1373, 1243, 981, 913, 838, 782, 732, 648 cm^{-1}; SEC (254 nm, THF): $M_{SEC} = 558$; PDI = 1.005.

Compound 5. Compound **4** (191 mg, 0.18 mmol), mono-TIPS-glutaric acid-HEG-OH (150 mg, 0.27 mmol), and DPTS (70 mg, 0.23 mmol) were dissolved in 2.0 mL of dichloromethane. DIPC (100 mg, 0.79 mmol) was added dropwise after 5 min. The reaction was complete after 4 h as determined by GPC, and removal of DPTS was achieved via four DI water extractions. The product was purified by column chromatography using 1:3 (v/v) hexane/EtOAc as an eluent ($R_f = 0.65$). Product (223 mg, 78% yield) was obtained as a colorless oil. ^{1}H NMR ($CDCl_3$) δ −0.30 (s, 3H)[c], −0.02 (s, 3H)[c], 0.80 (s, 9H)[c], 1.08 (broad, 18H)[a], 1.16 (m, 3H)[b], 1.21 (m, 3H), 1.82−1.98 (m, 9H), 2.15−2.20 (broad, 4H), 2.33−2.45 (m, 5H), 2.57 (broad, 4H), 3.67 (m, 22H), 3.85 (m, 2H), 3.95 (d, 1H), 4.23 (broad, 8H), 4.34 (d, 1H), 4.67 (s, 1H), 4.95 (d, 1H), 5.65 (t, 1H), 5.71 (m, 2H), 6.26 (broad, 2H), 7.09 (d, 1H), 7.33 (m, 3H), 7.42 (m, 4H), 7.52 (m, 3H), 7.62 (m, 1H), 7.75 (d, 2H), 8.13 (d, 2H). SEC (254 nm, THF): $M_{SEC} = 1110$; PDI = 1.002.

Compound 6. Compound **5** (100 mg, 62 μmol) was dissolved in 2.0 mL of THF. While the mixture stirred vigorously, 5.6 mL of glacial acetic acid were added. Last, 0.40 mL of DI H_2O was added dropwise, and the mixture was heated to 50 °C. TLC (1:3 mixture of hexane/EtOAc) shows the complete conversion of the carboxyl protected compound ($R_f = 0.65$) to the free carboxyl product ($R_f = 0.10$) after 12 h. The reaction was quenched by diluting the mixture with dichloromethane and washing several times with DI water. Precipitation from hexane gave 82 mg (91% yield) of isolated product. ^{1}H NMR ($CDCl_3$) δ −0.29 (s, 3H)[c], −0.02 (s, 3H)[c], 0.80 (s, 9H)[c], 1.21 (m, 3H), 1.82−1.98 (m, 9H), 2.15 (broad, 4H), 2.33−2.45 (m, 5H), 2.58 (broad, 4H), 3.66−3.70 (m, 24H), 3.95 (d, 1H), 4.23 (broad, 5H), 4.35 (d, 1H), 4.95 (d, 1H), 5.65 (t, 1H), 5.75 (m, 2H), 6.26 (broad, 2H), 7.11 (d, 1H), 7.33 (m, 3H), 7.43 (m, 4H), 7.52 (m, 3H), 7.62 (m, 1H), 7.75 (d, 2H), 8.13 (d, 2H); ^{13}C NMR (100 MHz, $CDCl_3$) δ −5.81, −5.17, 10.91, 12.29, 14.61, 17.70, 18.13, 19.62, 20.02, 20.73, 23.01, 23.40, 25.54, 26.38, 33.22, 42.32, 43.37, 46.84, 55.69, 56.04, 63.45, 69.14, 70.57, 71.30, 74.56, 75.07, 78.56, 80.99, 84.01, 126.42, 127.02, 128.00, 128.77, 129.17, 130.22, 131.87, 132.74, 133.71, 134.08, 138.20, 140.87, 166.87, 167.26, 168.96, 169.90, 171.51, 172.10, 172.97, 173.15, 201.98; IR (neat) ν_{max} 2958, 1733, 1662, 1520, 1451, 1372, 1259, 1108, 838, 802, 711 cm^{-1}; SEC (254 nm, THF): $M_{SEC} = 990$; PDI = 1.003.

Au(HEG-Paclitaxel-2′OTBS)$_n$ (7). Au(OH)$_n$ NPs (9.5 mg) were taken from a stock solution in *i*-propanol and dried on a rotary evaporator at 45 °C. The dried particles were then washed 3 times with dichloromethane to remove any residual isopropanol. 2′OTBS-Paclitaxel-7-GA-HEG-GA (20 mg, 14 μmol) and DPTS (12 mg, 40 μmol) were dissolved in 2.0 mL of dichloromethane and added to the vessel containing the dried hydroxyl-terminated nanoparticles. Please note that the Au(OH)$_n$ NPs are not soluble in CH_2Cl_2. Dropwise addition of 15 mg (0.12 mmol) of DIPC was done after 5 min, followed by addition of 1.0 mL of DMF to bring the Au(OH)$_n$ NPs into solution. The reaction was complete after 4 h as determined by GPC. DPTS and DMF were removed after several washes with DI water, and the remaining dichloromethane solution was evaporated on a rotary evaporator at 40 °C. The crude product was then dissolved in 10 mL of DMF and placed in a 30 kDa regenerated cellulose membrane filter. The sample was purified by ultracentrifugation at 3750 rpm until only one peak was observed by GPC (high molar mass peak). The solution was then concentrated *in vacuo* and precipitated from hexane, resulting in 27 mg of **7** in the form of a gray powder. ^{1}H NMR ($CDCl_3$) δ −0.30 (s, 3H)[c], −0.02 (s, 3H)[c], 0.80 (s, 9H)[c], 1.21 (m, 3H), 1.81−1.98 (m, 9H), 2.15 (broad, 5H), 2.30−2.50 (m, 9H), 2.58 (broad, 6H), 3.64−3.68 (m, 24H), 3.95 (d, 1H), 4.21 (broad, 5H), 4.35 (d, 1H), 4.95 (d, 1H), 5.65 (t, 1H), 5.75 (m, 2H), 6.26 (broad, 2H), 7.09 (d, 1H), 7.33 (m, 3H), 7.42 (m, 4H), 7.52 (m, 3H), 7.65 (m, 1H), 7.75 (d, 2H), 8.12 (d, 2H); ^{13}C NMR (100 MHz, $CDCl_3$) δ −5.50, −5.43, 10.66, 14.26, 18.01, 19.74, 20.12, 21.35, 22.76, 24.26, 25.37, 26.05, 32.77, 43.54, 46.70, 48.62, 54.80, 55.90, 56.66, 63.42, 68.84, 70.36, 70.82, 71.51, 74.73, 75.09, 75.93, 77.23, 78.68, 79.01, 79.34, 80.46, 83.60, 127.56, 128.01, 128.26, 128.57, 128.76, 130.06, 130.40, 131.28, 133.17, 133.46, 135.08,

138.84, 140.35, 165.70, 166.92, 169.13, 170.70, 171.80, 172.02, 172.75, 202.06; IR (neat) ν_{max} 3446, 2951, 1733, 1634, 1539, 1484, 1398, 1126, 895, 839, 711 cm^{-1}; SEC (254 nm, THF): $M_{SEC} = 10\,500$; PDI = 1.02.

Au(HEG-Paclitaxel)$_n$ (8). Au(HEG-Paclitaxel-2′OTBS)$_n$ (27 mg) was dissolved in 1.5 mL of THF and transferred to a small polypropylene vial. While the mixture stirred, 0.50 mL of HF in pyridine (70:30, respectively) was added (Please note that safe laboratory practices should be observed when handling HF). The deprotection was quenched after 4 h by diluting the reaction mixture with dichloromethane and washing several times with DI water. The organic fraction was reduced and washed thrice with hexane, yielding 25 mg of a gray powder. ^{1}H NMR ($CDCl_3$) δ 1.15−1.19 (m, 7H), 1.80−2.00 (m, 14H), 2.15 (s, 4H), 2.20−2.50 (m, 13H), 2.51−2.70 (broad, 3H), 3.63−3.80 (m, 24H), 3.91 (d, 1H), 4.21−4.28 (broad, 7H), 4.93 (d, 1H), 5.55 (t, 1H), 5.65 (d, 1H), 5.75 (d, 1H), 6.20 (broad, 2H), 7.15 (broad, 1H), 7.32−7.62 (m, 12H), 7.75 (d, 2H), 8.10 (d, 2H); ^{13}C NMR (100 MHz, $CDCl_3$) δ 11.14, 11.51, 14.28, 20.63, 20.98, 21.95, 23.03, 25.54, 25.92, 26.61, 32.01, 32.79, 44.07, 47.34, 56.44, 57.17, 63.99, 67.91, 69.39, 70.92, 71.65, 74.96, 75.28, 75.72, 76.37, 77.77, 80.94, 84.03, 128.10, 128.36, 128.94, 129.37, 130.59, 130.96, 132.03, 133.63, 134.11, 135.54, 140.46, 141.15, 166.24, 167.32, 169.73, 171.15, 172.39, 173.34, 173.72, 202.68; IR (neat) ν_{max} 3418, 3061, 2955, 2359, 2342, 1734, 1654, 1602, 1580, 1522, 1483, 1370, 1236, 1107, 802, 715, 668 cm^{-1}; SEC (254 nm, THF): $M_{SEC} = 7000$; PDI = 1.05.

Acknowledgment. The authors gratefully acknowledge the financial support provided by the National Science Foundation (DMR-0547399 and CBET-0506832) and Robert A. Welch Foundation (L-C-003).

Supporting Information Available: ^{1}H NMR and ^{13}C NMR spectra of intermediate compounds, additional GPC traces and calibration curve, FTIR, and DLS data. This material is available free of charge via the Internet at http://pubs.acs.org.

JA075181K

Supporting Information

Paclitaxel-Functionalized Gold Nanoparticles

Jacob D. Gibson, Bishnu P. Khanal, Eugene R. Zubarev

Department of Chemistry, Rice University, Houston, Texas 77005

E-mail: zubarev@rice.edu

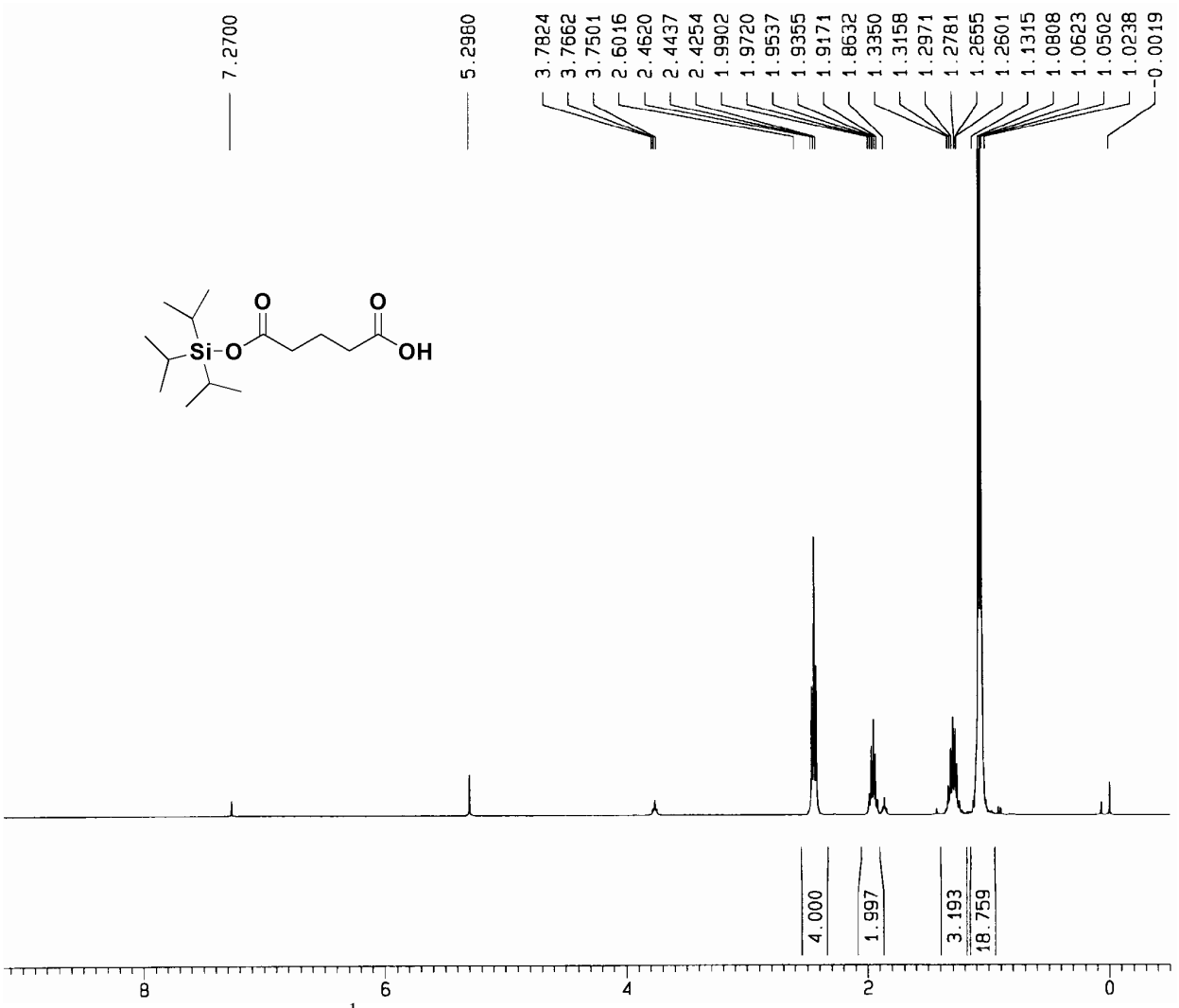

Figure S1. ^{1}H NMR spectrum of TIPS-protected glutaric acid.

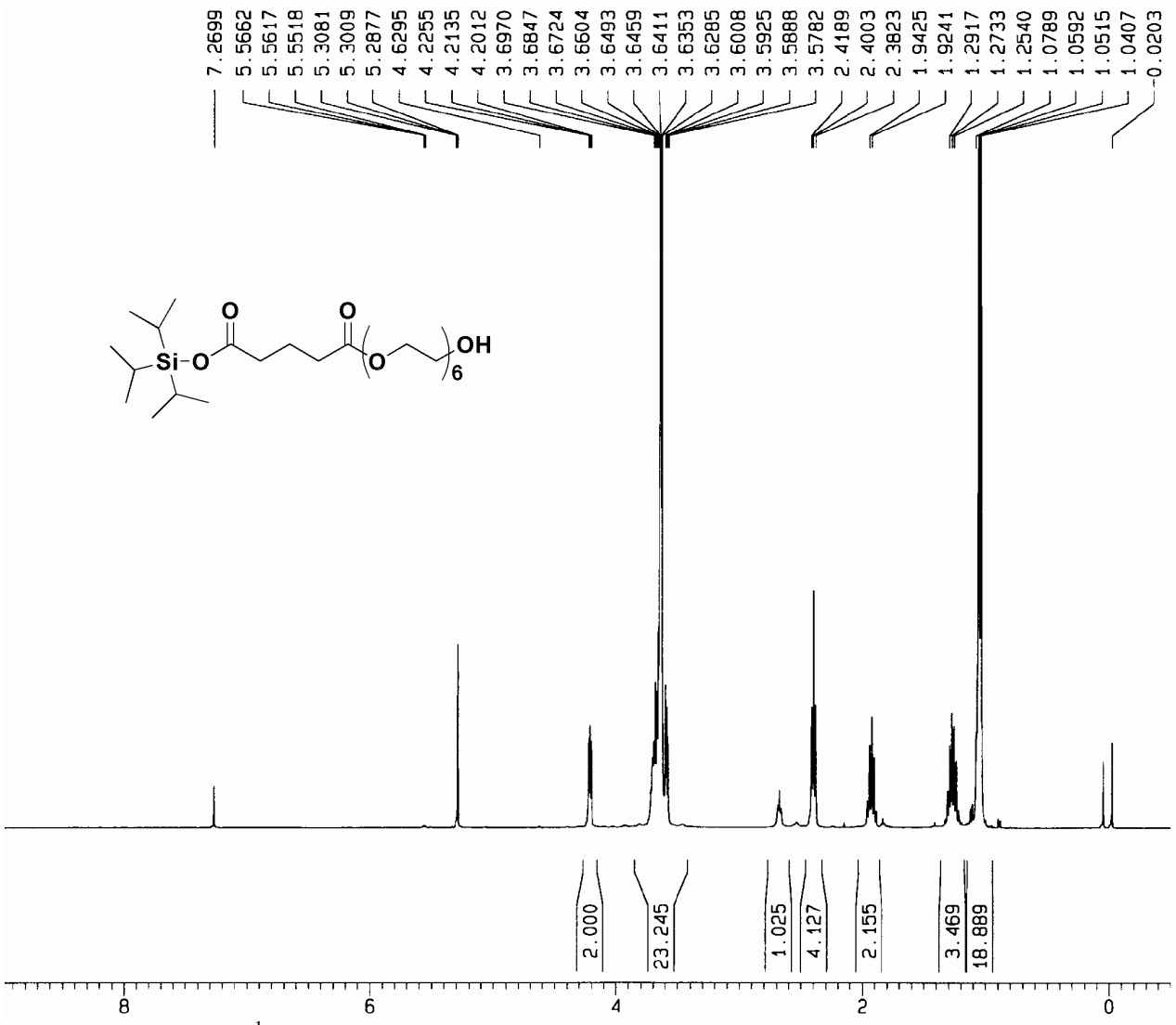

Figure S2. ^{1}H NMR spectrum of TIPS-protected hexaethylene glycol glutarate.

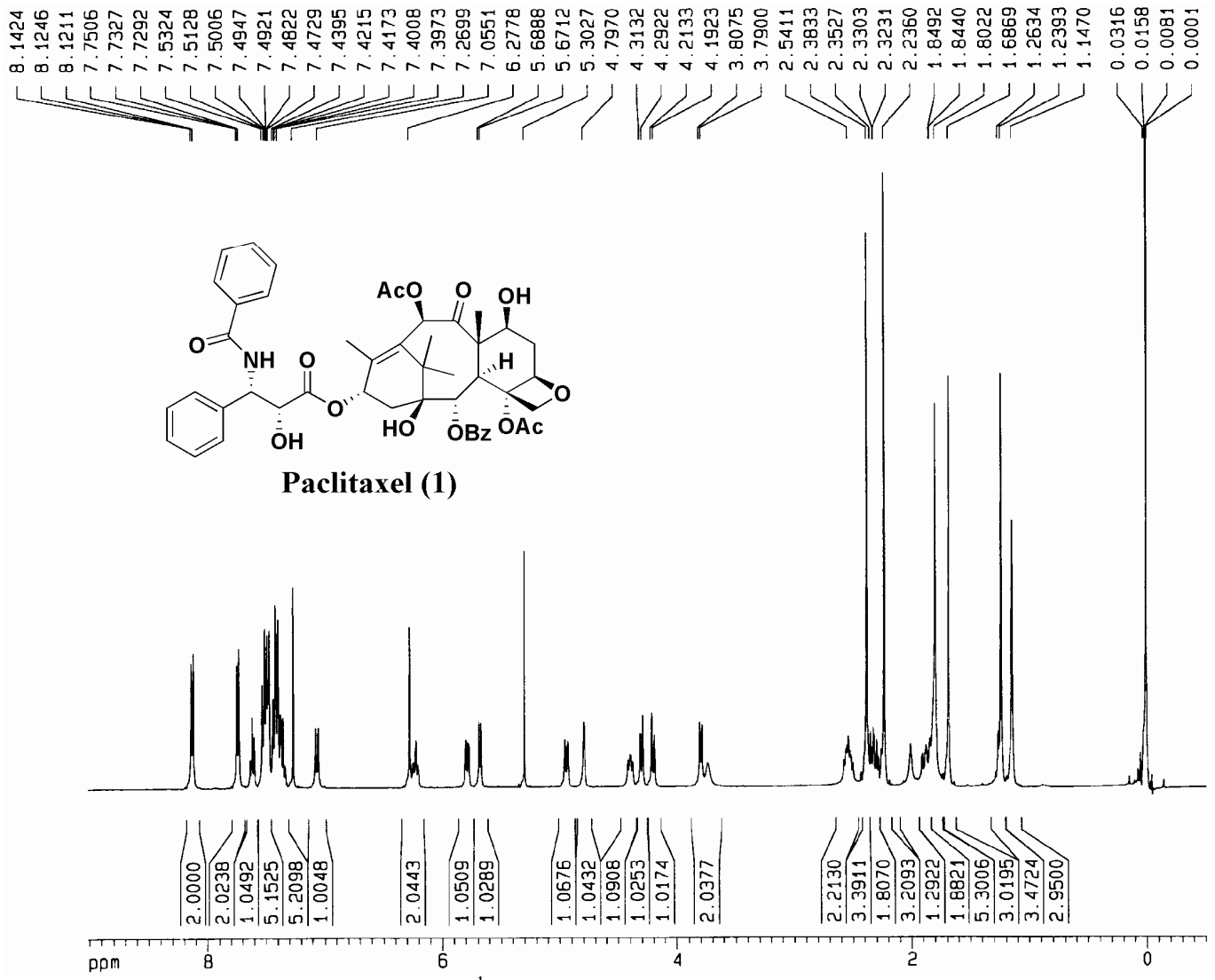

Figure S3. ^{1}H NMR spectrum of paclitaxel **1**.

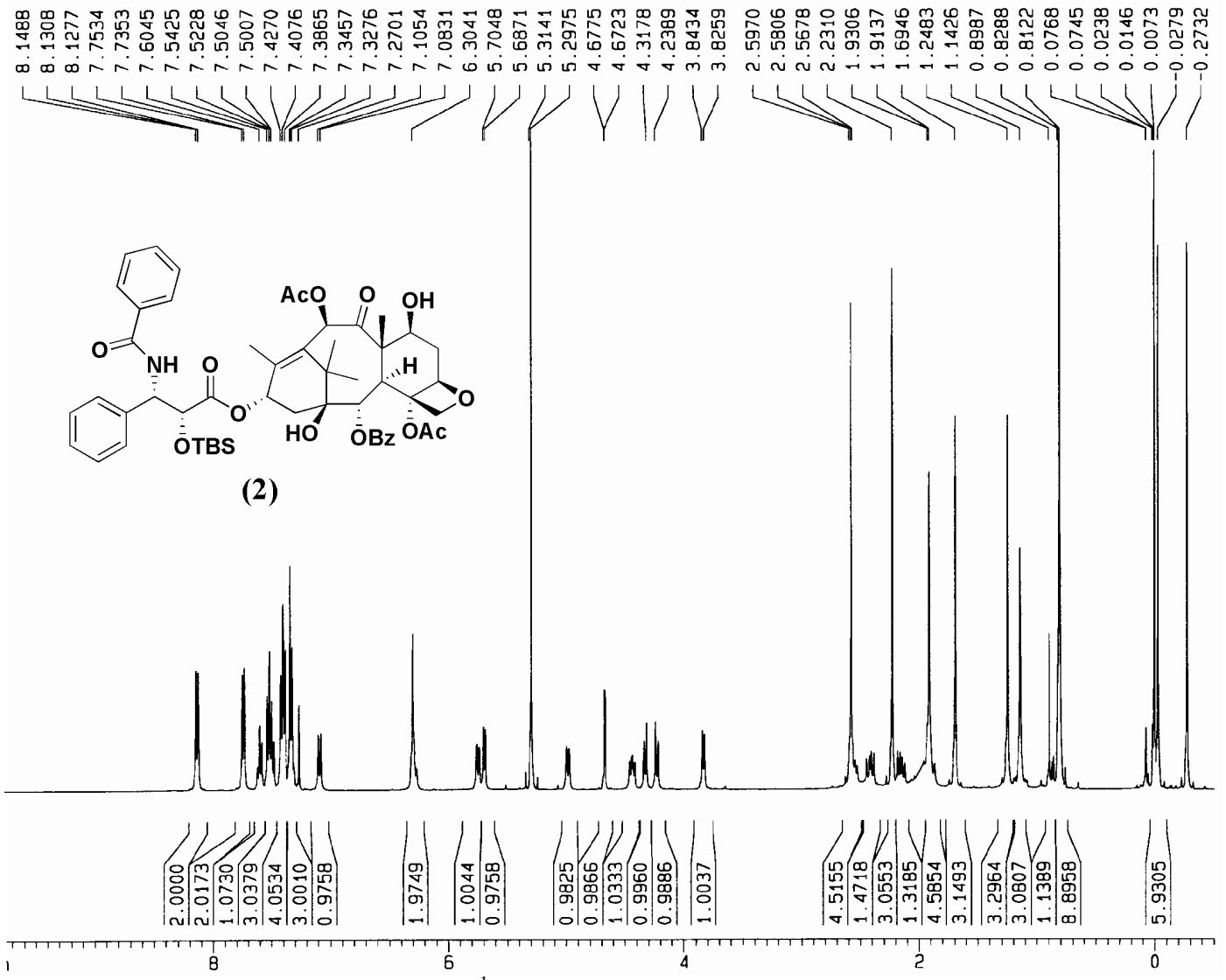

(2)

Figure S4. ^{1}H NMR spectrum of compound **2**.

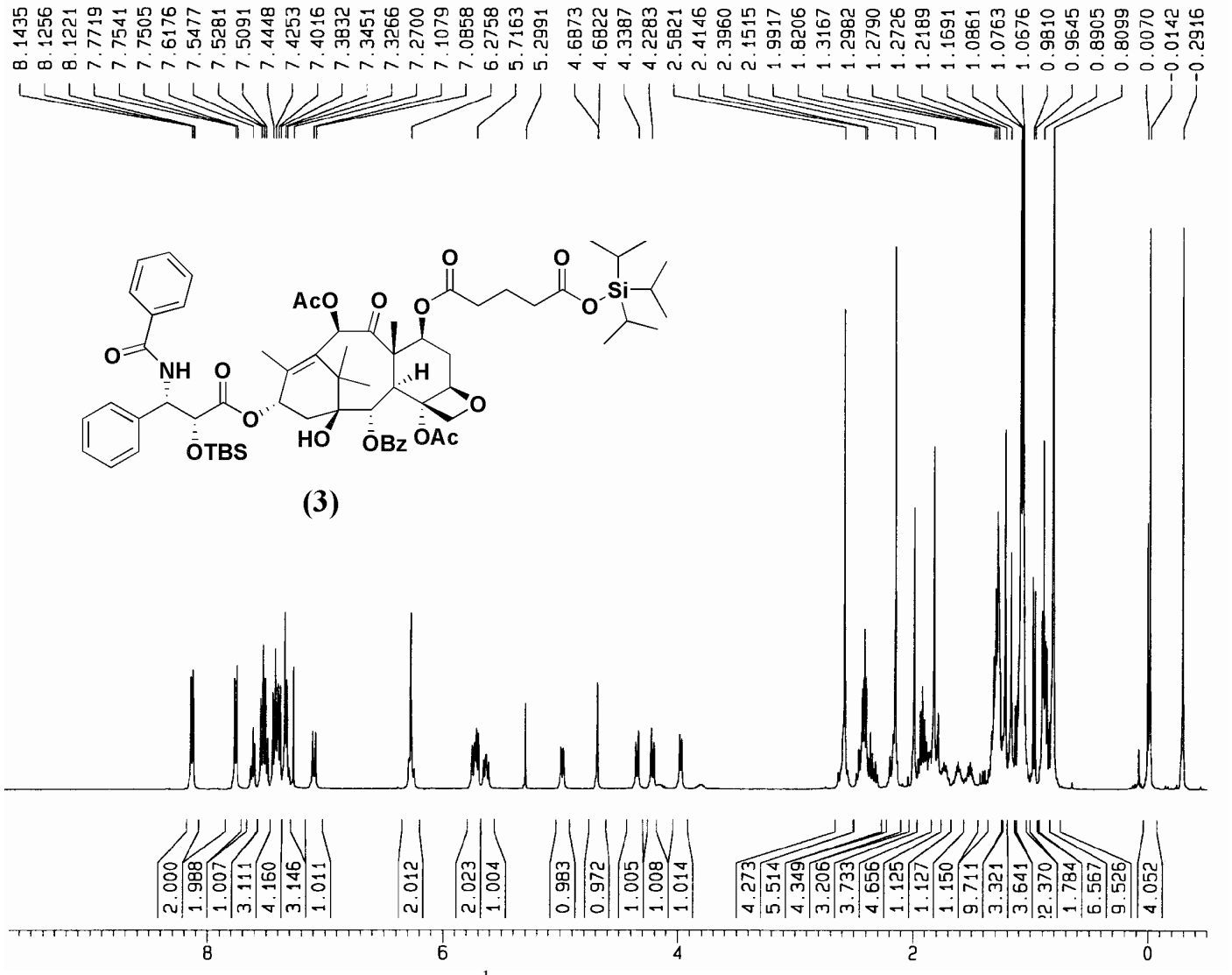

(3)

Figure S5. ^{1}H NMR spectrum of compound **3**.

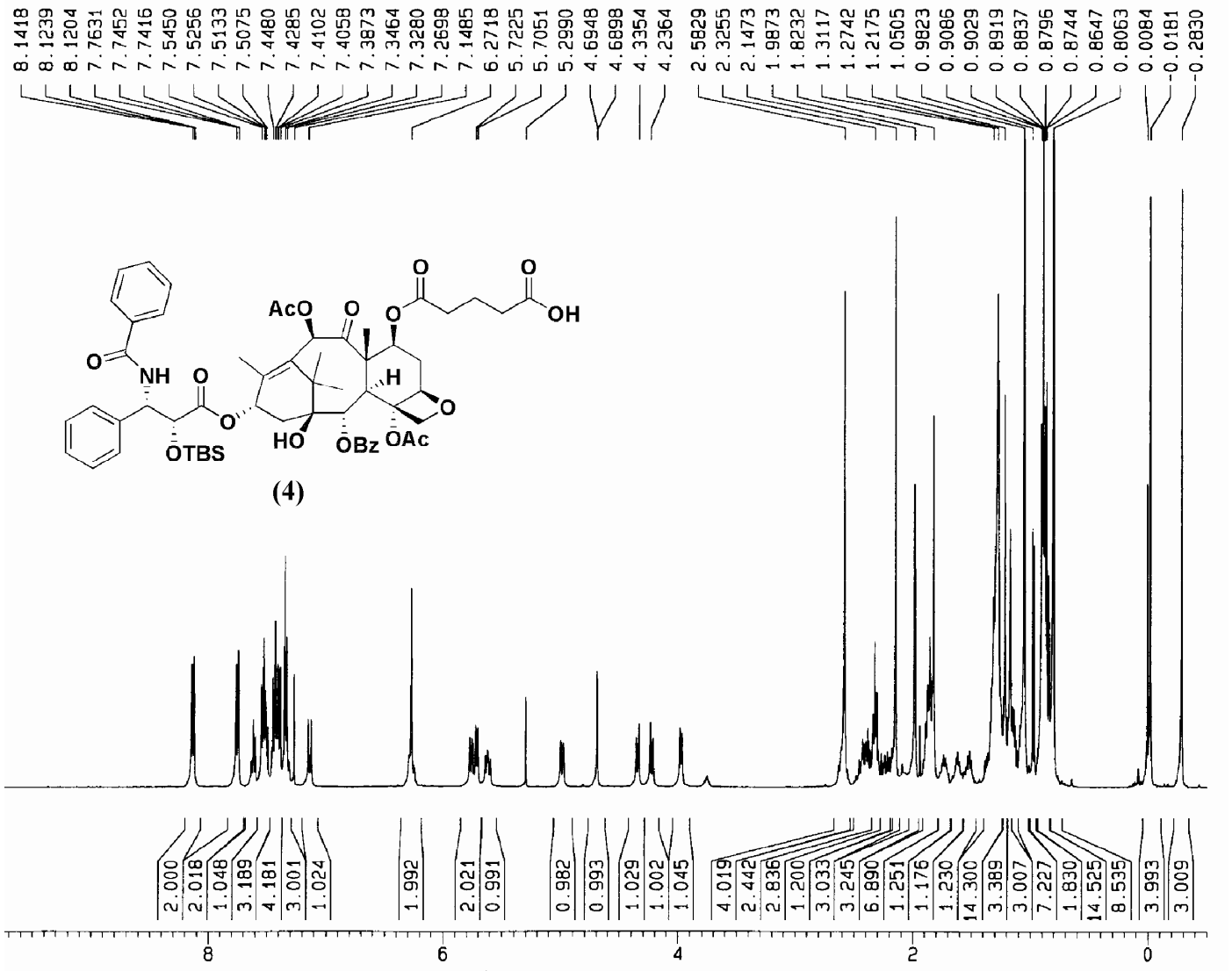

(4)

Figure S6. ^{1}H NMR spectrum of compound **4**.

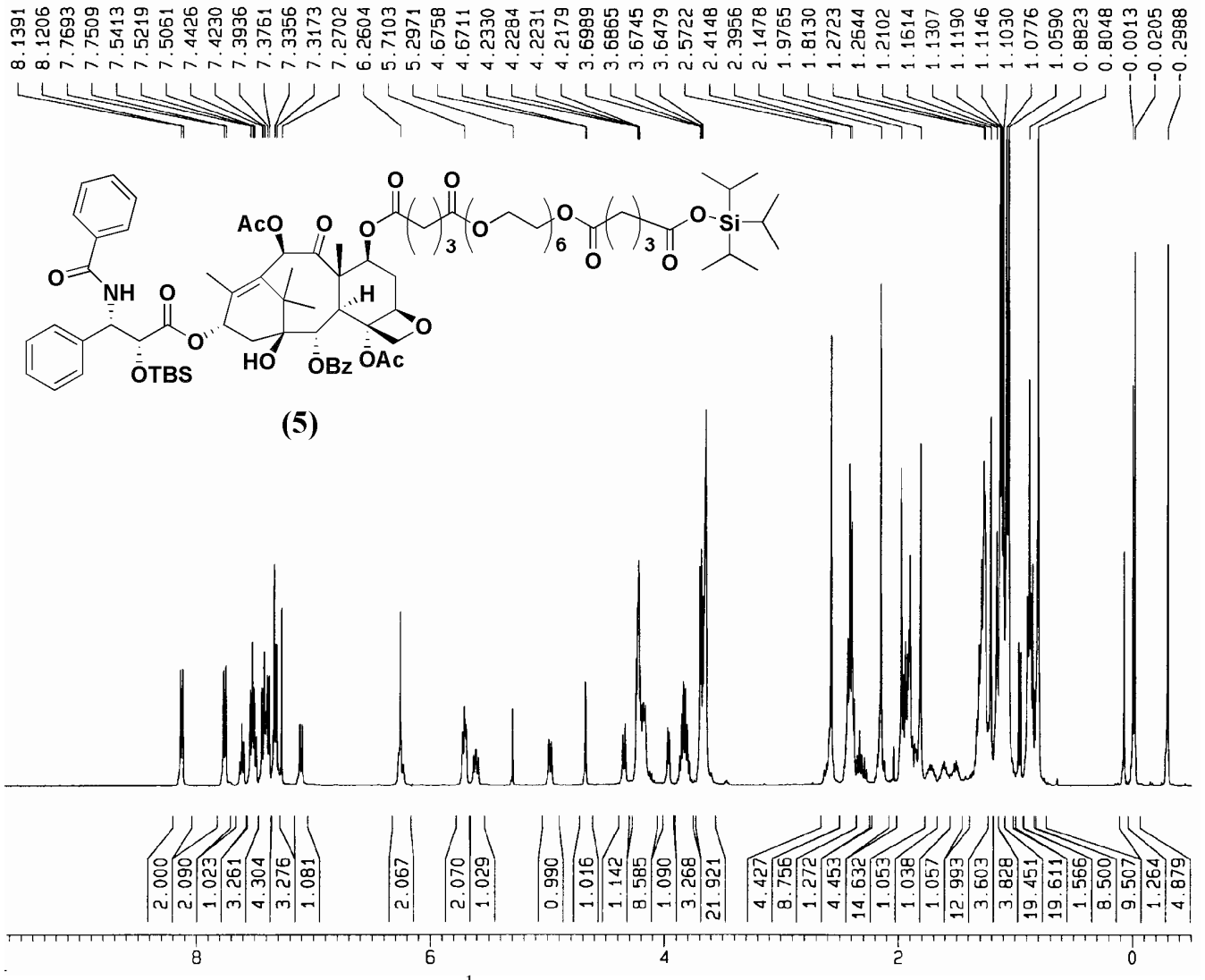

Figure S7. ^{1}H NMR spectrum of compound **5**.

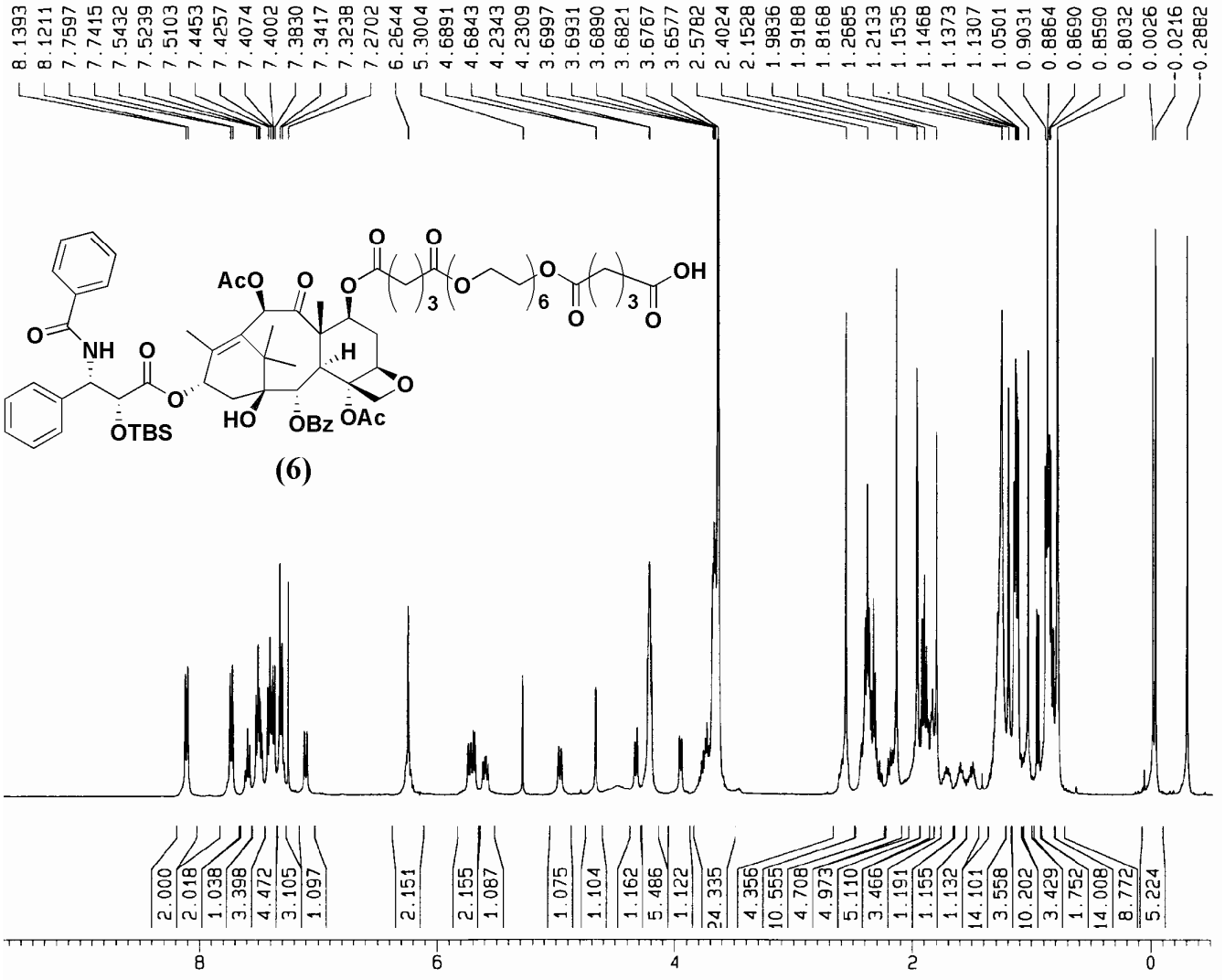

(6)

Figure S8. ^{1}H NMR spectrum of compound **6**.

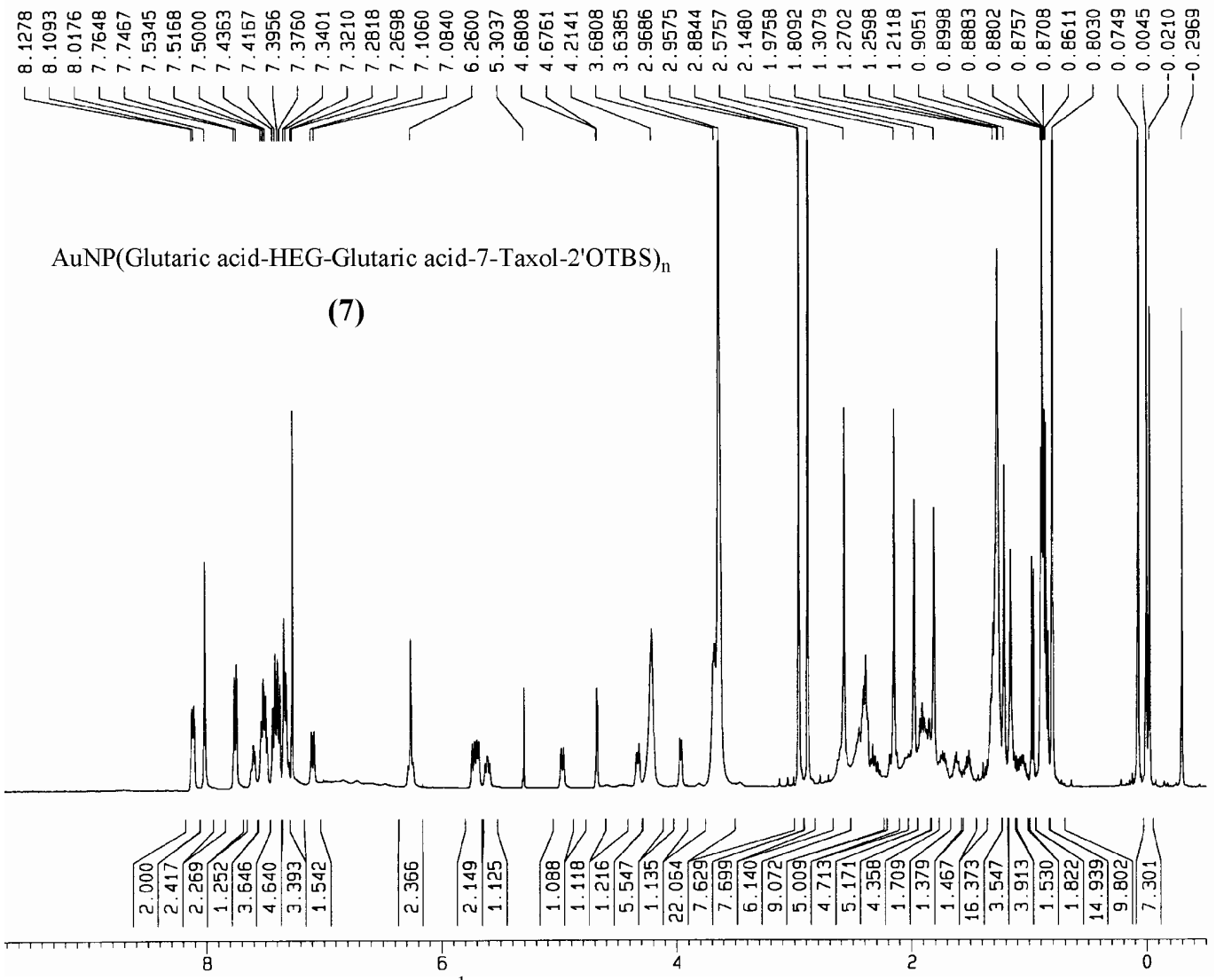

Figure S9. ^{1}H NMR spectrum of nanoparticles **7**.

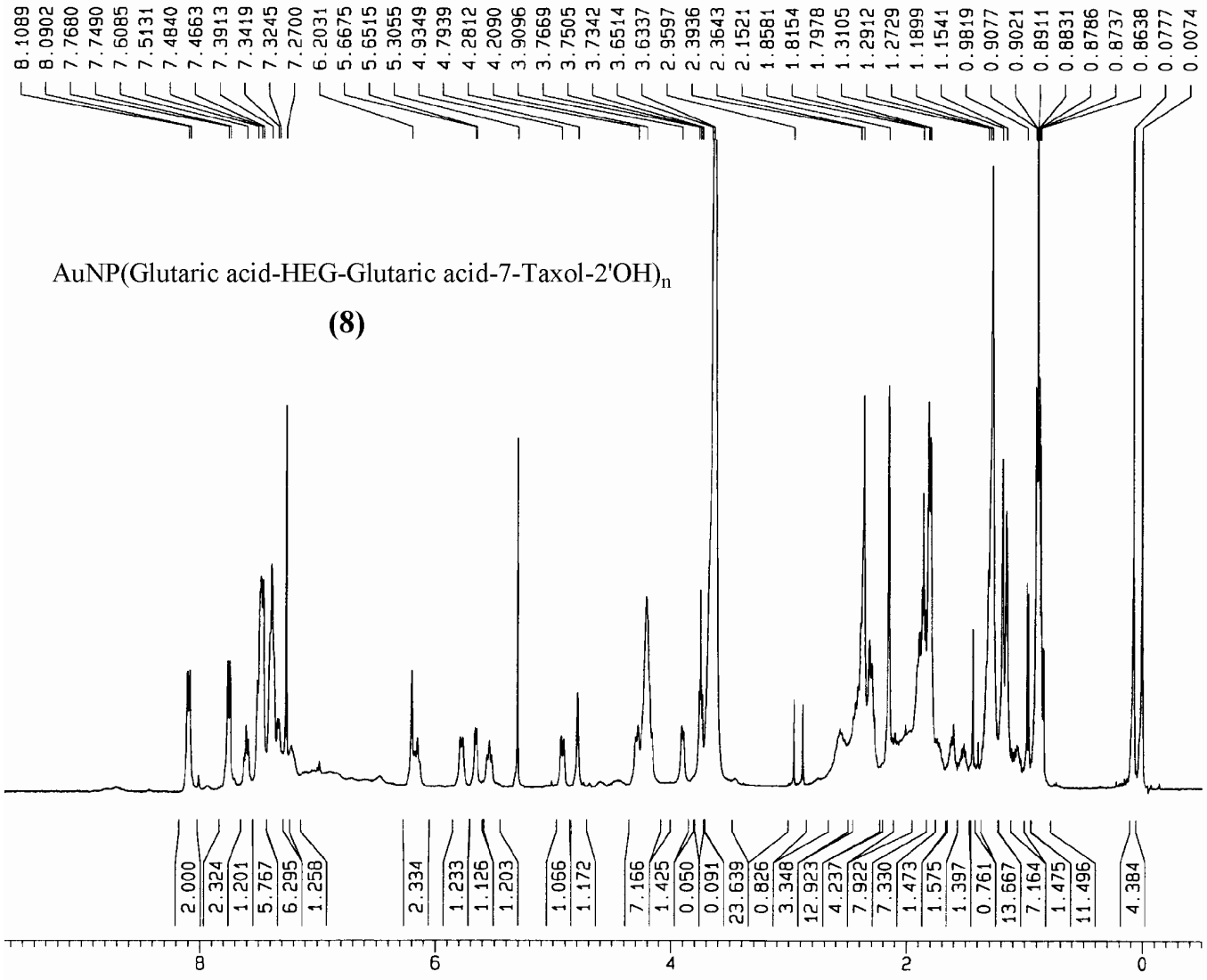

Figure S10. ^{1}H NMR spectrum of nanoparticles **8**.

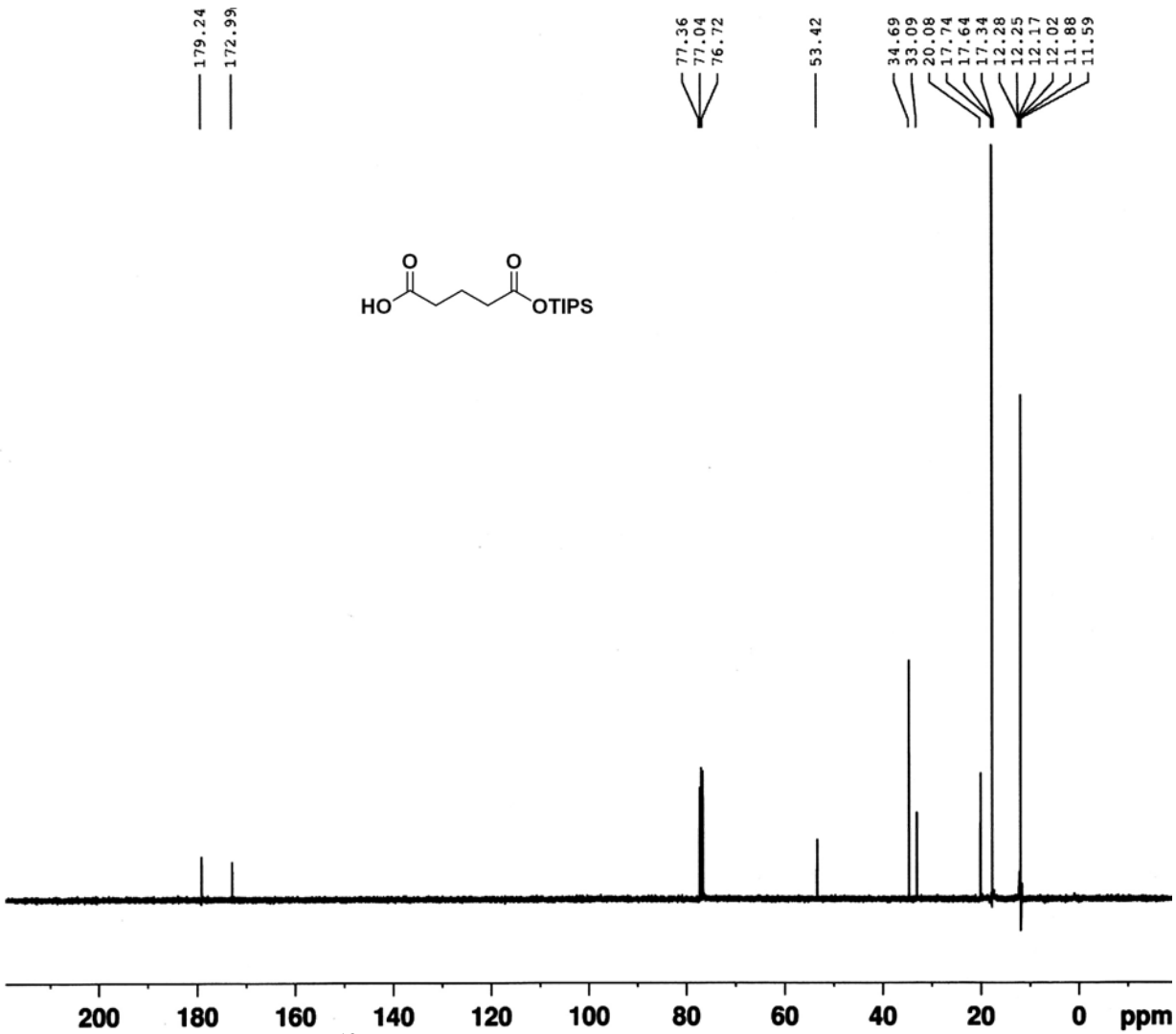

Figure S11. ^{13}C NMR spectrum of TIPS-protected glutaric acid.

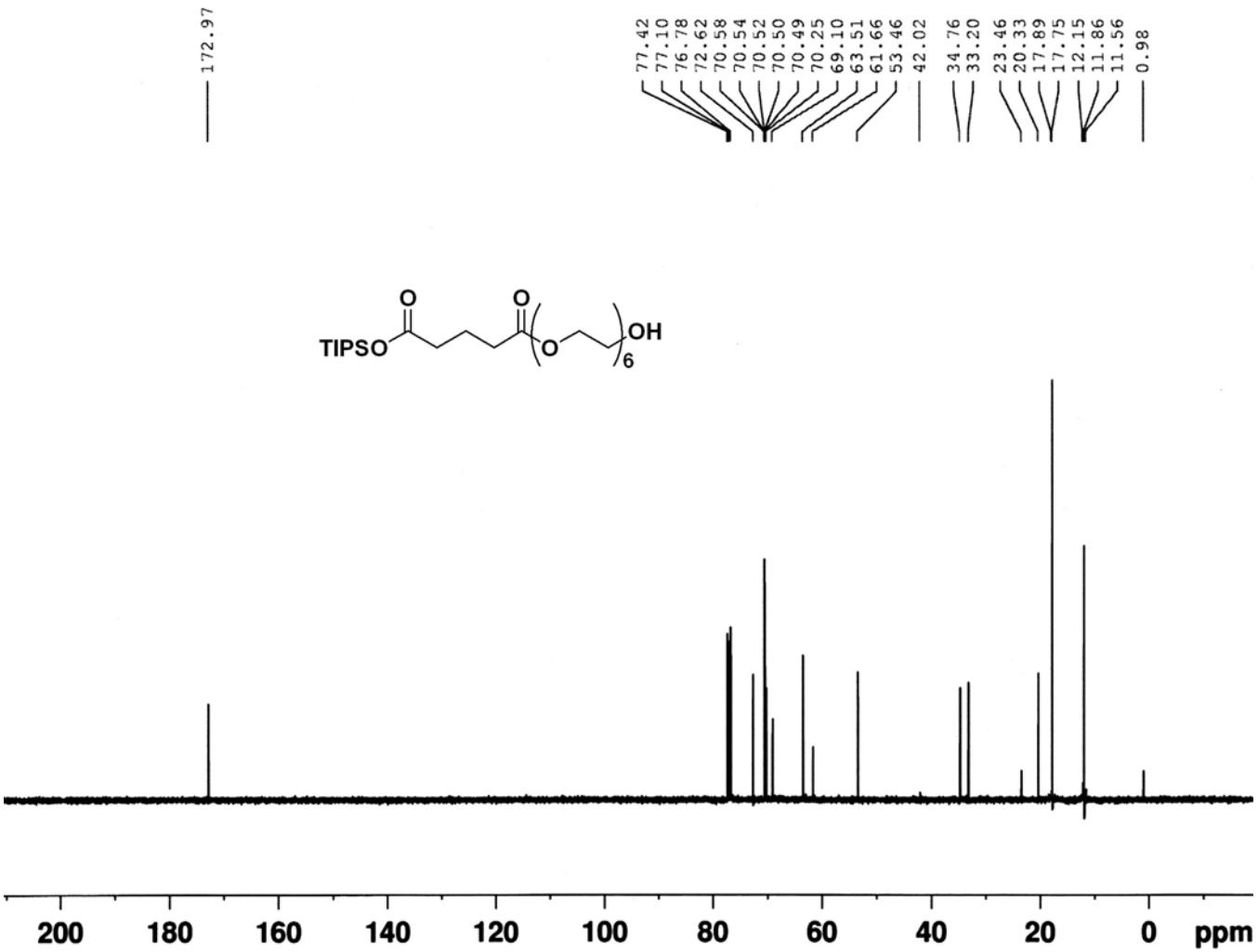

Figure S12. ^{13}C NMR spectrum of TIPS-protected hexaethylene glycol glutarate.

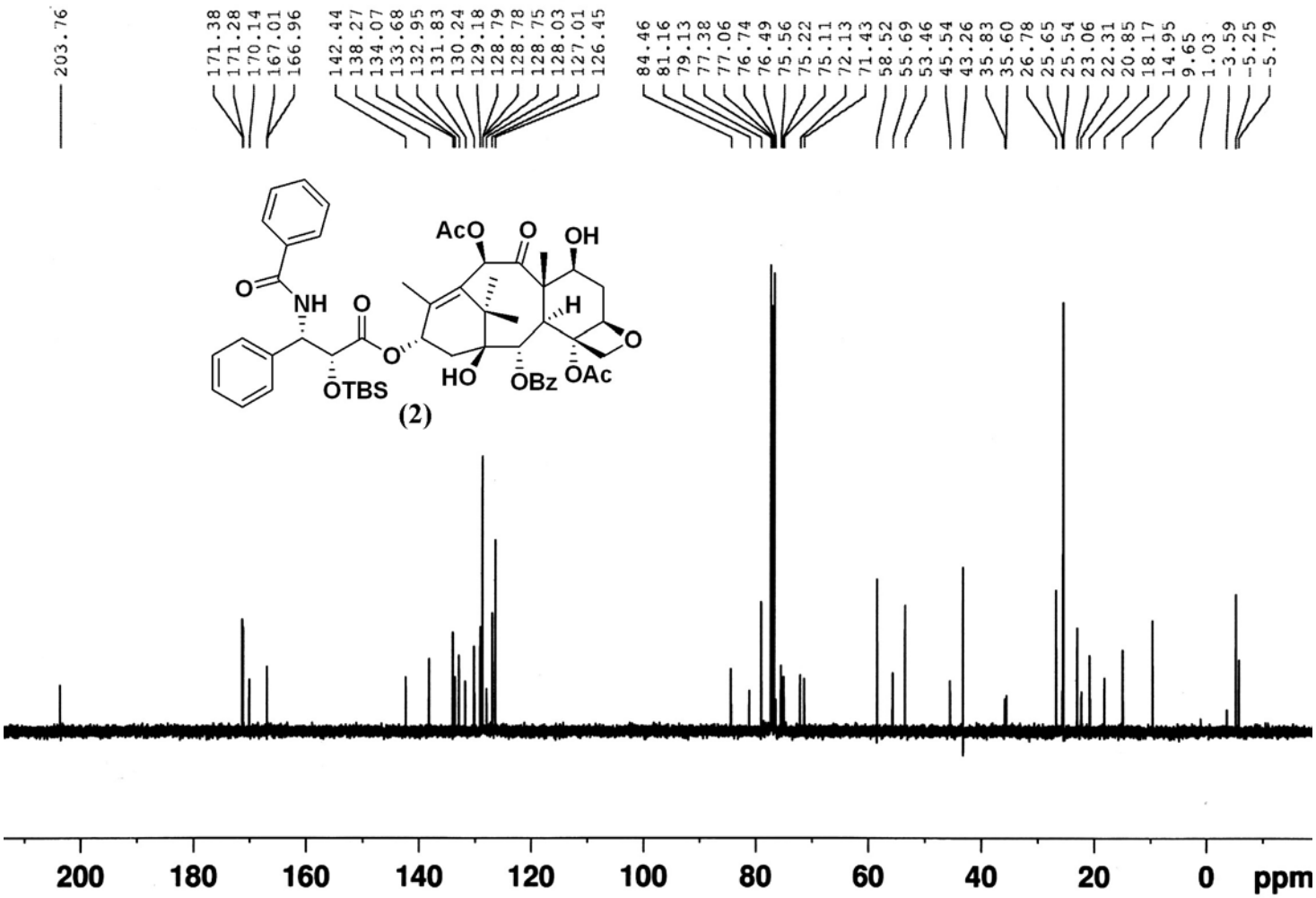

Figure S13. ^{13}C NMR spectrum of compound **2**.

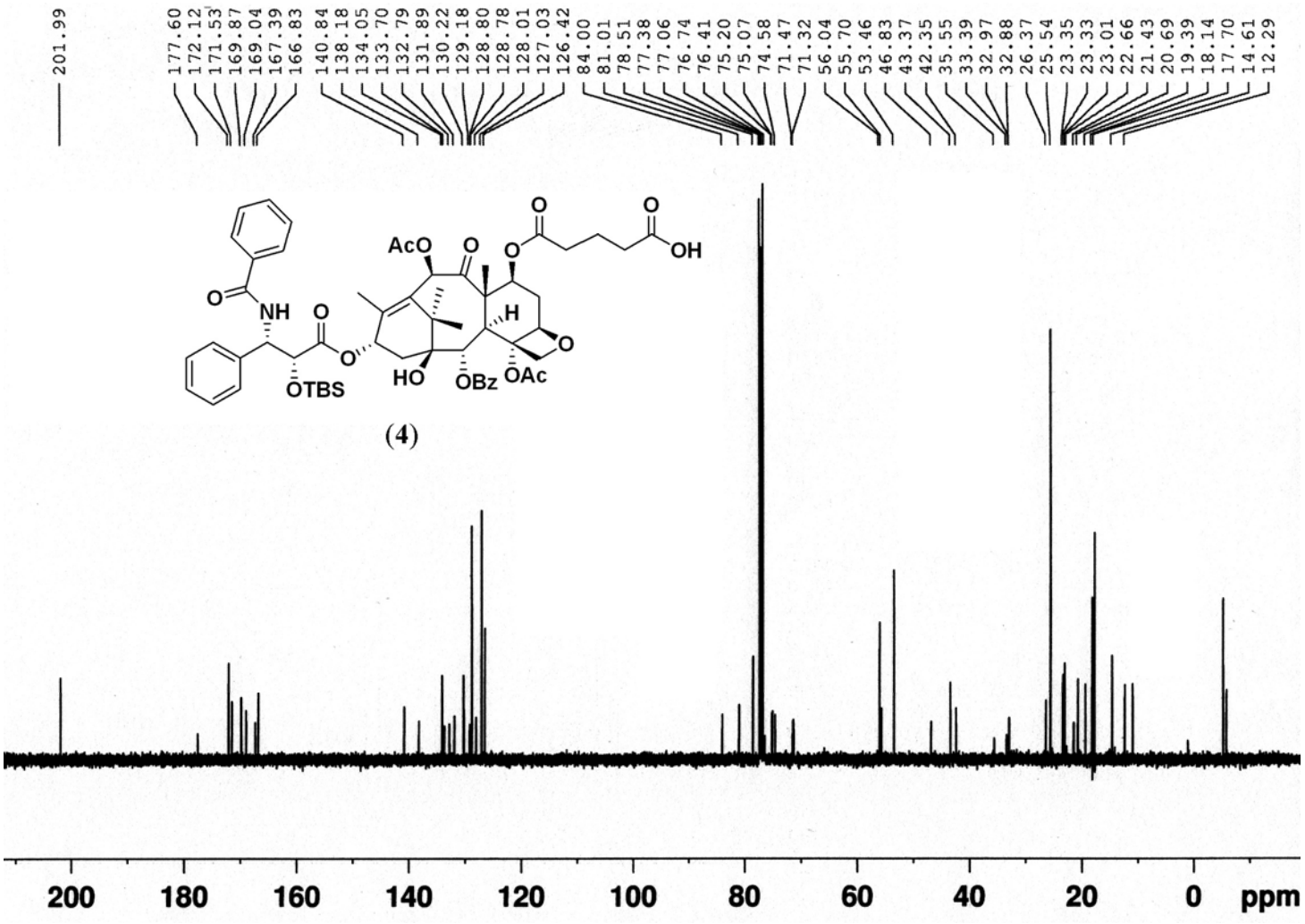

Figure S14. ^{13}C NMR spectrum of compound **4**.

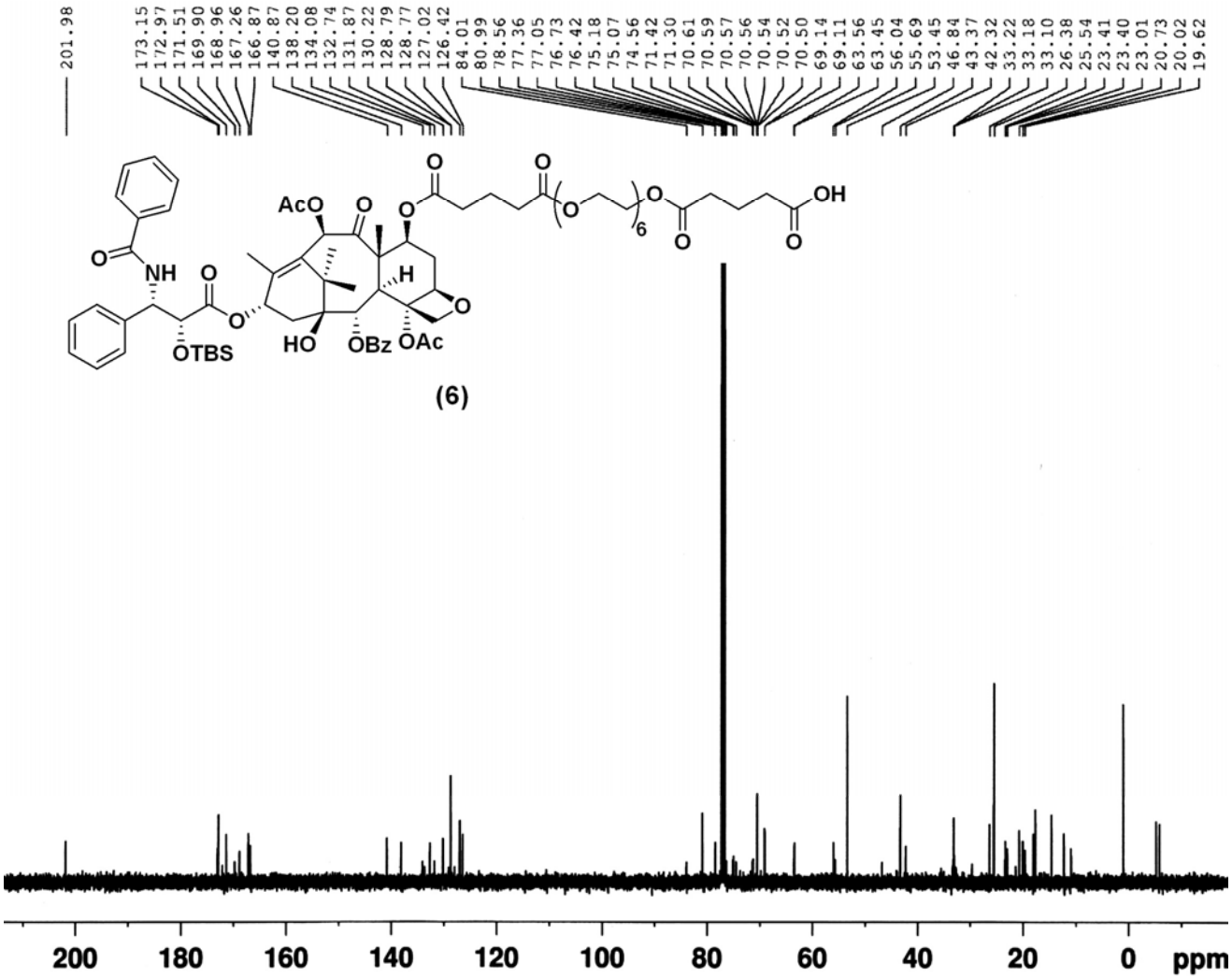

Figure S15. ^{13}C NMR spectrum of compound **6**.

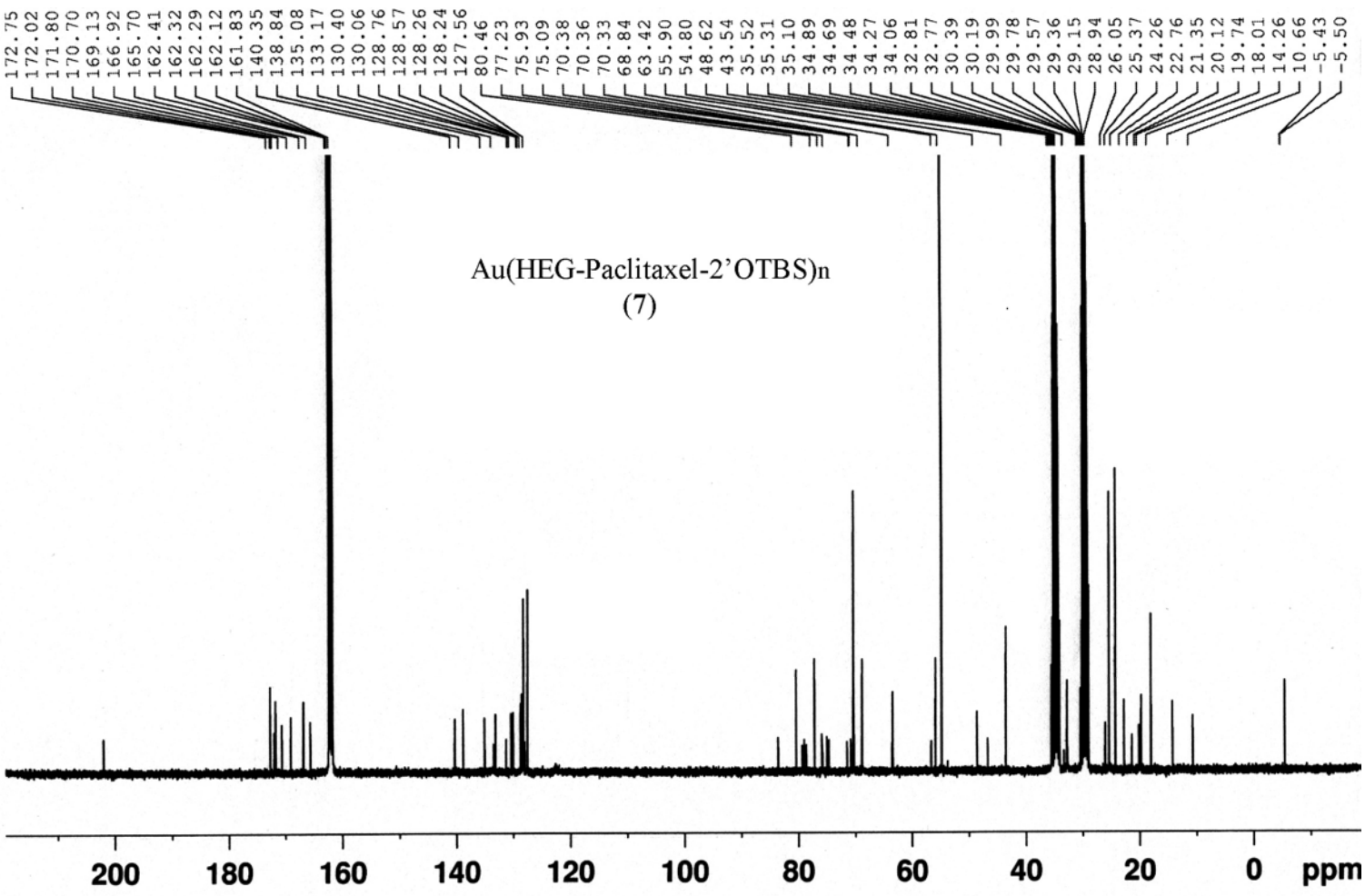

Figure S16. ^{13}C NMR spectrum of nanoparticles **7**.

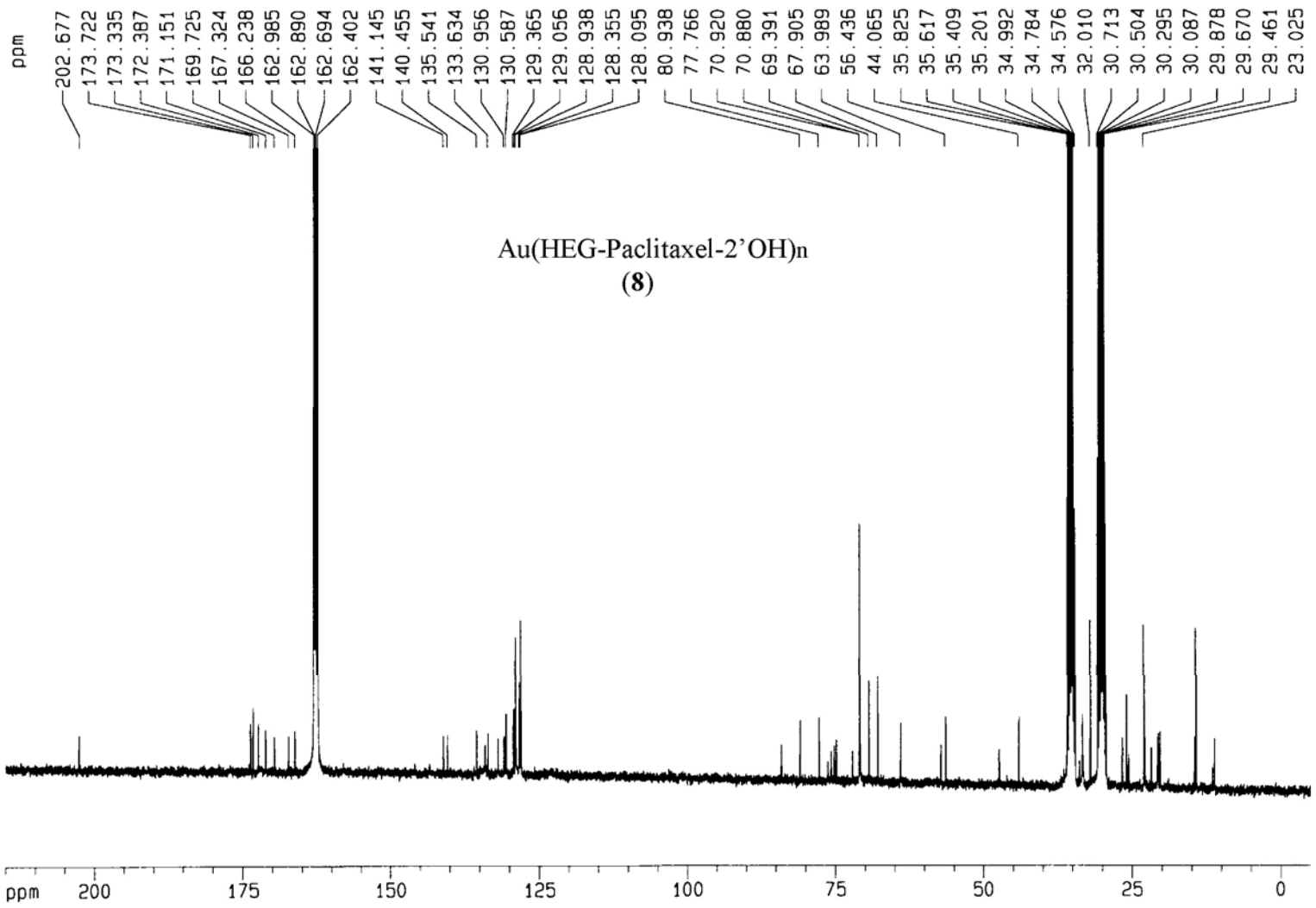

Figure S17. ^{13}C NMR spectrum of nanoparticles **8**.

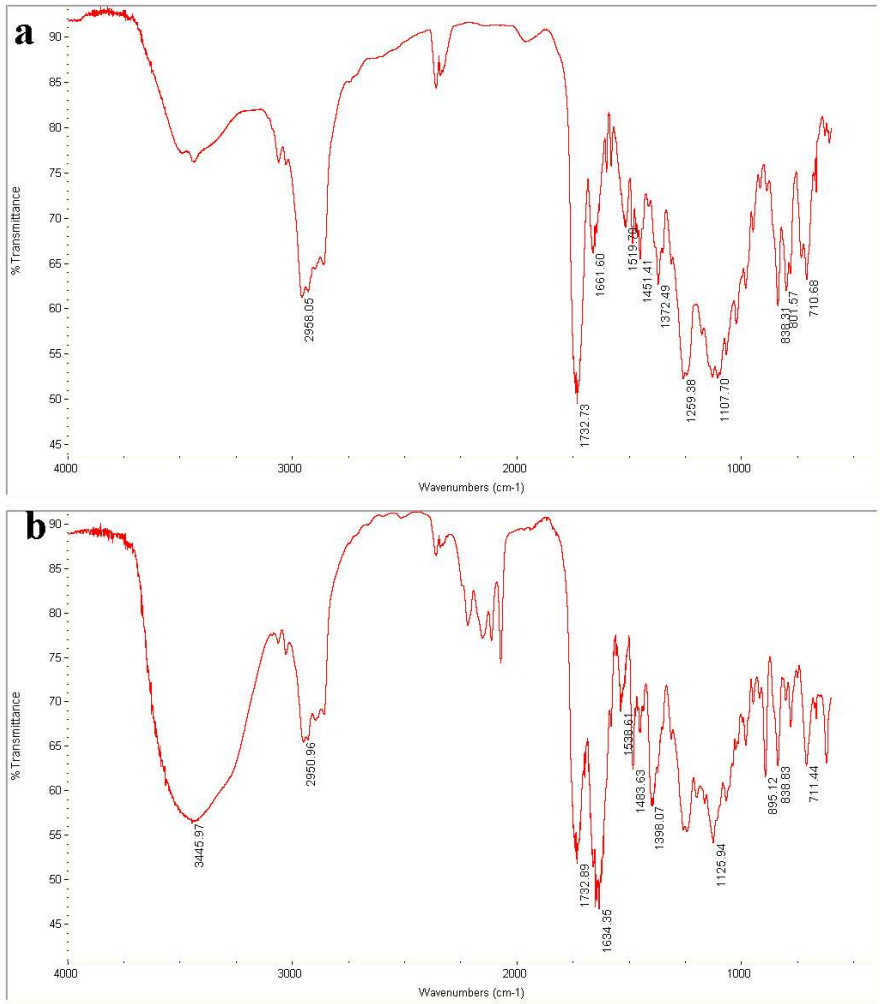

Figure S18. IR spectra of compound **6** (a) and the isolated nanoparticles **7** (b).

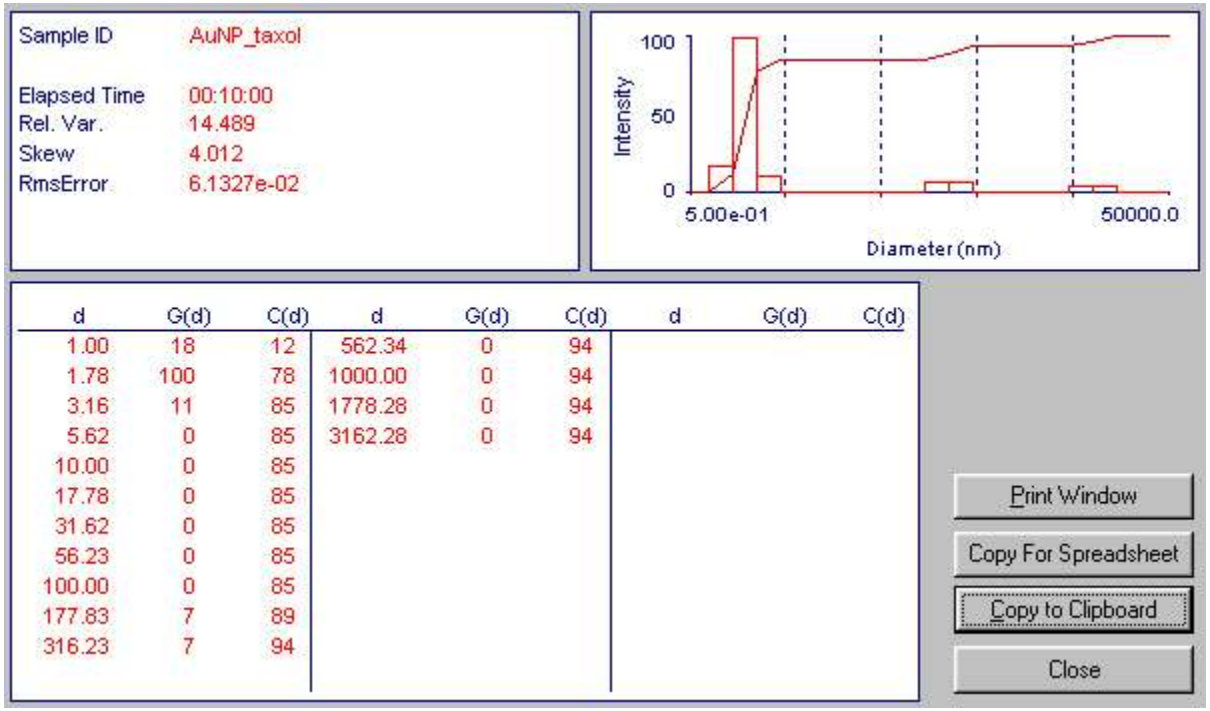

Figure S19. Dynamic light scattering (DLS) data collected from a THF solution of nanoparticles **8**. The average diameter is 1.8 nm, which is close to the size of the nanoparticles gold core as determined by TEM. The size distribution is very narrow and in good agreement with the GPC data (see Fig. 1 in the main text, and Fig. S22).

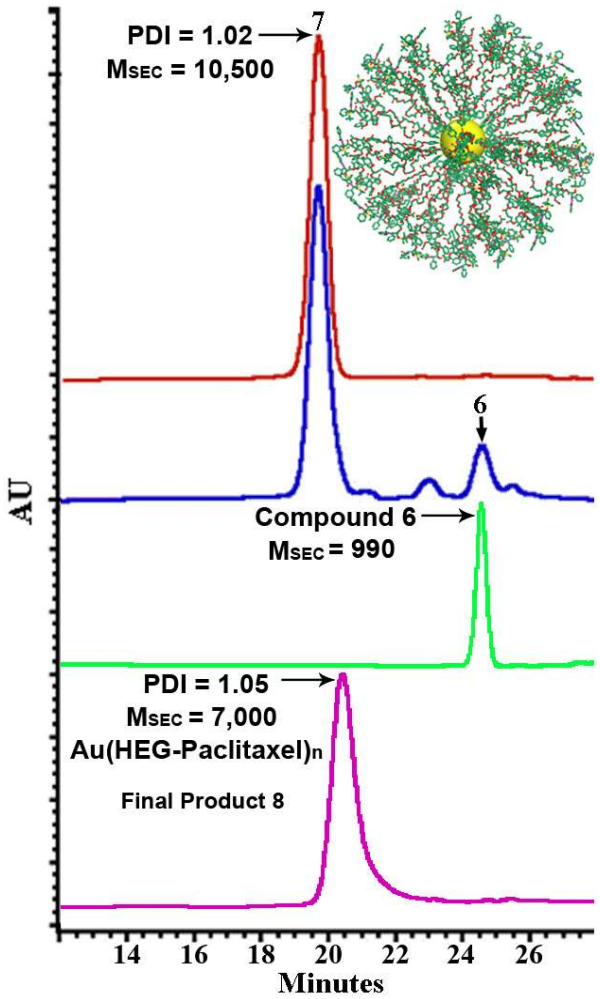

Figure S20. GPC traces of purified nanoparticles **7** (red), reaction mixture after 2 h coupling of compound **6** to mercaptophenol-coated Au NPs (blue), pure compound **6** (green), and the purified final product **8** (magenta).

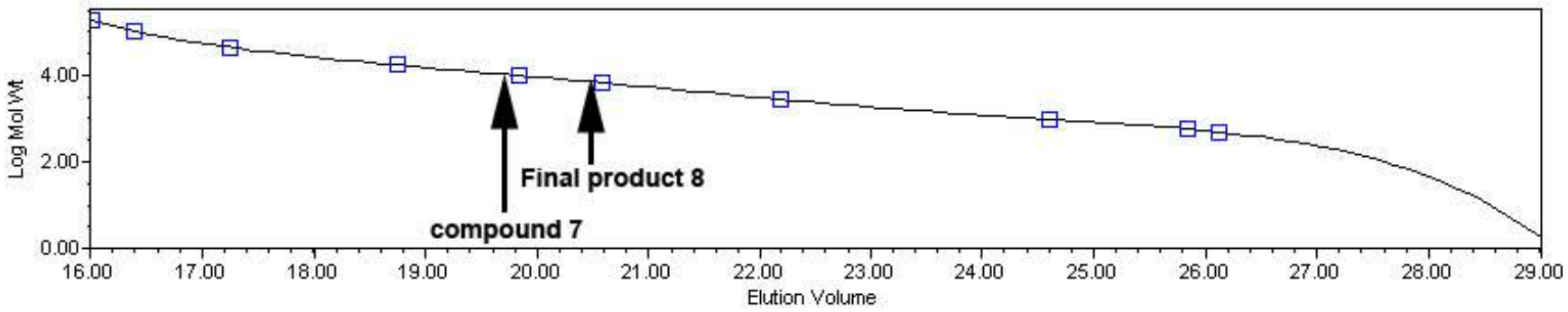

Figure S21. GPC calibration curve based on linear polystyrene standards. Note that both nanoparticles **7** and **8** elute at retention times (19.7 and 20.47 min, respectively), which are far away from the exclusion limit of the columns.